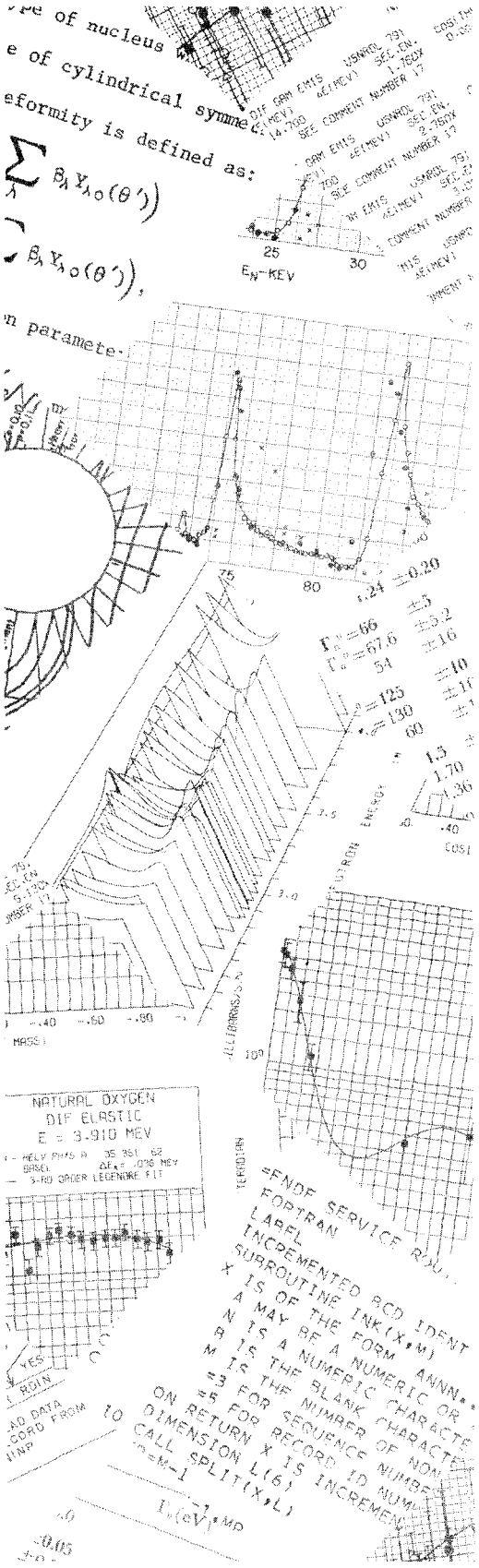

STERN

BNL-NCS-50593
(ENDF-246)

EVALUATION OF CHROMIUM NEUTRON AND GAMMA PRODUCTION CROSS SECTIONS FOR ENDF/IV

A. PRINCE

August 1976

INFORMATION ANALYSIS CENTER REPORT

NATIONAL NEUTRON CROSS SECTION CENTER
BROOKHAVEN NATIONAL LABORATORY
UPTON, NEW YORK 11973

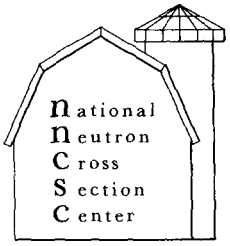

BNL-NCS-50593
(ENDF-246)
(Physics, Nuclear - TID-4500)

EVALUATION OF CHROMIUM NEUTRON AND GAMMA PRODUCTION CROSS SECTIONS FOR ENDF/IV

A. PRINCE

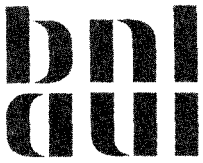

August 1976

NATIONAL NEUTRON CROSS SECTION CENTER
BROOKHAVEN NATIONAL LABORATORY
ASSOCIATED UNIVERSITIES, INC.
UNDER CONTRACT NO. EY-76-C-02-0016 WITH THE
UNITED STATES ENERGY RESEARCH AND DEVELOPMENT ADMINISTRATION

Printed in the United States of America
Available from
National Technical Information Service
U.S. Department of Commerce
5285 Port Royal Road
Springfield, VA 22161
Price: Printed Copy $6.00; Microfiche $3.00

January 1977 600 copies

Table of Contents

List of Figures

List of Tables

I. Introduction:

Chromium, along with iron and nickel constitutes the main components of the cladding and structural materials used in fast reactors. The description of the nuclear data for these materials plays a very important role in predicting the characteristics of fast power reactors. This has caused the fast reactor and shielding physicist to demand greater accuracy in the data sets recommended for neutronics and photonics calculations.

While experimental techniques have improved in the past few years, there are still large discrepancies between the various measurements, not to mention the numerous gaps that exist in the empirical data.

In an effort to minimize the uncertainties and to fill the gaps where data do not exist, the Evaluated Nuclear Data File periodically updates its files so as to include the latest refinements.

In keeping with this policy, an updating of the CR-ENDF/III cross section library was undertaken.

The previous evaluation of Cr was given the MAT (MATerial number) 1121 and is described in File 1 (ENDF/B-III) and Reference 1.

This report describes a re-evaluation for Cr for ENDF/IV (MAT 1191).

II. General:

The most important data for the structural materials are the scattering cross sections, in particular the inelastic neutron cross sections and their energy distributions.

The following sections will outline the various experimental data used in this evaluation and also outline some of the theoretical concepts that were used to predict the various cross sections in regions where experimental data were non-existent.

Table 1 shows a comparison of ENDF/III (MAT 1121) and ENDF/B-IV (MAT 1191) for Cr.

Tables 2 to 5 depict the possible neutron induced reactions and their respective Q values for the four stable isotopes of chromium (^{50}Cr, ^{52}Cr, ^{53}Cr, ^{54}Cr) for energies $E \leq 20.0$ MeV.

Also included in these tables are the percent abundance, mass and binding energy for each isotope.

III. Compilation of Experimental Data

A. Resonance Region

Resonance data now exist up to about 600 keV for the chromium isotopes.[2] For ^{50}Cr and ^{52}Cr resonance information extends to 591 keV and 530 keV respectively, while for ^{53}Cr and ^{54}Cr data are available up to 246 keV and 394 keV.

The capture widths are not as well known and information exists only for energies below 150 keV with the majority of these widths being determined by the capture area method giving $g \frac{\Gamma_n \Gamma_\gamma}{\Gamma}$. The total cross sections in the resonance region are rather complete with the major portion coming from the Duke,[3,4,5] Karlsruhe,[6,7] and RPI[8] results. Unlike the total cross section, the radiative capture cross section in the resonance region is not well known. Several measurements exist at the thermal energy thus defining rather substantially this value, where extra-

polation with a 1/v dependence is the usual method for estimating $\sigma_{n\gamma}$ for energies up to about 600 eV. In the keV region the absolute capture cross section in the energy range 70 keV to 550 keV has been reported by C. LeRigoleur et al., at a Karlsruhe meeting, May 1973. Other point data or interval averaged capture cross sections exist up to about 200 keV.

B. Fast Neutron Region

1. Total Cross Section

Starting at about 500 keV and extending to beyond 30 MeV, very accurate high resolution measurements have been carried out for σ_T on natural Cr.[9-12] The most recent experimental data has been reported by ORNL.[13] Data on the separated isotopes ^{52}Cr and ^{53}Cr exist from 2.5 to 15.0 MeV[14] while only a few data points exist for ^{50}Cr and ^{54}Cr, the most recent being at 14.2 MeV[15] where σ_T was measured for all four isotopes.

The observed behavior of σ_T within the isotopic chain showed a difference of about 4% for the heaviest (^{54}Cr) and the lightest (^{50}Cr) isotopes.

2. Elastic Cross Section

The most information on the experimental data for σ_{el} consists of the work of Holmqvist and Wiedling[16] and most recently ORNL,[17] who have just completed measurements for Cr(Nat.) and ^{52}Cr up to 8.56 MeV. Several isolated points spanning the region 2.5 to 15.0 MeV may also be found in the CINDA/CSISRS compilation.

3. Radiative Capture

Practically no measurements exist in the region 1 MeV to 10 MeV. Most evaluations in the radiative capture cross sections are normalized to the 14.1 MeV value of Cvelbar et al.[18] Since the capture cross section is so small compared to the other reaction cross section, it is not deemed critical to have a lack of measurements in the high energy region.

4. $\sigma_{n,p}$

Only a very small number of experiments exist for the n,p reaction in the Cr isotopes and most of these are centered about 14 MeV. The most recent measurements using the neutron activation process have been reported by B. T. Kenna and P. E. Harrison[19] for $^{50,52,53,54}Cr$. For ^{52}Cr Kern[20] et al., have carried out measurements from 12 to 18 MeV.

5. $\sigma_{n,\alpha}$

Up until recently only one measurement existed for this reaction and this was for ^{54}Cr.[21] Recently, data at 14.7 MeV for $^{50,52,53,54}Cr$ have been reported at Kiev (1973) by Dolya et al.[22] These values have been used in the ENDF/B-IV evaluation for Cr(Mat.).*

6. $\sigma_{n,2n}$

Except for ^{52}Cr[23] and ^{50}Cr[24] the literature shows that only a few isolated points between 14 and 15 MeV exist for

*Since the completion of the evaluation another measurement has been reported for the (n,α) reaction at 14.7 ± 0.3 MeV for ^{54}Cr by S. M. Qaim at the 167th National Meeting of the American Chemical Society, Los Angeles, Calif., March 31, 1974.

this region. Recent measurements have been reported in references 19, 25, 26, and 27.

7. $\sigma_{n,3n}$

No data reported. Due to the high threshold, no significant contribution is anticipated for this particular reaction below 20.0 MeV.

8. $\sigma_{n,t}$

Hardly any data exists for this reaction, however, due to its small magnitude (σ < 200 μ b around 15 MeV) it is not deemed highly important. Qaim et al.[26,28] have recently reported a value of 66 ± 20 μb at 14.6 MeV which is consistent with expectations.

9. Other Reactions

Reactions with emission of charged particles such as n,d; n,pn; n,n He^4; etc. have practically no reported experimental data. A few isolated points for $\sigma_{n,np}$ for ^{52}Cr and ^{53}Cr have been reported at 15.0 MeV (see CINDA 1973). This lack of experimental information will lead to some difficulty in predicting recommended values obtained from nuclear theory or systematics.

10. $\sigma_{n,n'}$

The inelastic scattering cross section with the emission of gamma rays is of great importance; however, the amount of experiment data for natural Cr and its isotopes is scarce and spotty. The early measurements of Van Patter,[29] Broder,[30] Kiehn,[31] and Degtyarev[32] provide experimental data on $\sigma_{n,n'}$

and $\sigma_{n,n'\gamma}$ spectra up to about 4.0 MeV, however, these data exhibit uncertainties up to 30%. Recently Kinney and Perey[17] have reported measurements up to 8.56 MeV for Cr(Nat.) and ^{52}Cr. Other new measurements have been reported in References 33 to 42 and/or CINDA (1973) and CSISRS.

In Figures 1 to 4 a set of bar graphs are given so that one may see at a glance where experimental data are lacking for n,particle reactions. Information in the resonance region is not included on the graph. The heavy black lines indicate measurements which are separated by approximately 1.0 MeV or less. The dashed lines indicate isolated measurements and the dots indicate a measurement(s) at one particular energy. Although it is possible to assume that the elastic or non-elastic cross section is known when either of these exist along with the total cross section, they are not shown on the bar graph. The energy threshold for a certain reaction is indicated by a vertical line, the absence of which indicates an exoergic reaction. In the case of neutron-charged particle reactions, the effect of the Coulomb barrier is not considered.

A combination of the experimental data and theoretical concepts using nuclear model codes was used to analyze all possible neutron cross sections in the range from 10^{-5} eV to 20.0 MeV.

IV. Theoretical Analysis

In order to fill the gaps in the experimental data especially for the differential and total elastic scattering and the inelastic scattering cross section, it was necessary to carry out theoretical

calculations using several nuclear model codes. The starting point for such an analysis was the optical model which was used to provide the total cross section σ_T, the shape elastic cross section σ_{SE} and the compound nucleus (reaction cross section) σ_R.

Two computer codes were used for these calculations, namely ABACUS,[43] which treated the Cr isotopes as spherical and a modified version of JUPITOR[44] in which a deformed potential could be employed to describe the collective excitations.

To describe the compound nuclear reactions such as compound elastic σ_{CE}, compound inelastic $\sigma_{nn'}$ (discrete and continuum), and radiative capture $\sigma_{n\gamma}$ the nuclear model codes COMNUC[45] and FISPRO[46] were employed. The remaining reaction cross sections, such as $\sigma_{n,2n}$; $\sigma_{n,3n}$; $\sigma_{n,p}$; $\sigma_{n,d}$; $\sigma_{n,t}$; $\sigma_{n,\alpha}$ etc. (see Tables 2 - 5) were calculated using the empirical model code THRESH.[47]

The results of these various codes were combined in a consistent manner so that adequate agreement with the existing experimental data was achieved.

Once their criteria were satisfied, the acquired prescription was used to predict the various cross sections in areas lacking empirical data.

A brief description of the analytical procedures involved in these calculations follows.

A. Optical Model

The potential used in the optical model calculations had the conventional form given by

$$V(r) = - V_R f(R_R a_R r) - iW_v f(R_I a_I r) + i4a_I W_s f'(R_I a_I r)$$

$$+ V_{s.o.} \left(\frac{\hbar}{m_\pi c}\right)^2 \frac{1}{r} f'(R_{s.o.} a_{s.o.} r) \vec{\sigma} \cdot \vec{l},$$

where

$$f(R_i a_i r) = \left[1+\exp \frac{r-R_i}{a_i}\right]^{-1} \qquad (1)$$

V_R = depth of the real potential

W = depth of the imaginary potential (v = vol., s = surf.)

V_{so} = depth of the spin-orbit potential

R_R = radius of the real nuclear potential

R_I = radius of the imaginary nuclear potential

a_R = diffuseness parameter of the real potential

a_I = diffuseness parameter of the imaginary potential

a_{so} = diffuseness parameter of the spin-orbit potential

π = pion mass

σ = Pauli's spin operator

l = orbital angular momentum operator

In order to obtain the contribution of the direct inelastic scattering component, a vibrational model undergoing dynamic deformations about a spherical shape was assumed. Thus the radius in equation 1 was expressed as

$$R = R(\theta,\phi) = R_o \left[1 + \sum_{\lambda\mu} \alpha_{\lambda\mu} Y_{\lambda\mu}(\theta,\phi)\right] \qquad (2)$$

where

$\alpha_{\lambda\mu}$ may be described in terms of the deformation parameter β.[48]

The Optical Model Parameters derived for the chromium isotopes are given below (all E in MeV)

^{52}Cr

$V_R = (50.9617 - 0.574\ E)$ MeV

$W_S = (6.18 + 0.4195\ E + 0.0089E^2)$ MeV

$W_V = (0.0)$ MeV

$V_{so} = (7.35)$ MeV

$r_R = (1.2647 - 0.00527\ E)$ fm

$r_s = (1.3202 - 0.00527\ E)$ fm

$r_{so} = r_R$

$a_R = (0.7692 - 0.00528\ E)$ fm

$a_s = (0.4638 - 0.00318\ E)$ fm

$a_{so} = a_R$

^{50}Cr

$V_R = (51.6137 - 0.584\ E)$ MeV

$W_s = (6.2984 + 0.4192 + 0.0086\ E^2)$ MeV

$W_V = (0.0)$ MeV

$V_{so} = (7.6)$ MeV

$r_R = (1.2584 - 0.0037\ E)$ fm

$r_s = (1.3142 - 0.0037\ E)$ fm

$r_{so} = r_R$

a_R = (0.7640 - 0.005 E) fm

a_s = (0.4628 - 0.003 E) fm

$a_{so} = a_R$

$\underline{^{54}Cr}$

V_R = (48.8352 - 0.544 E) MeV

W_S = (5.871 + 0.4217 E + 0.0099 E^2) MeV

W_V = (0.0) MeV

V_{so} = (6.89) MeV

r_R = (1.2658 - 0.0039 E) fm

r_s = (1.3210 - 0039 E) fm

$r_{so} = r_R$

a_R = (0.7756 - 0.00564 E) fm

a_s = (0.4660 - 0.0034 E) fm

$a_{so} = a_R$

$\underline{^{53}Cr}$

V_R = (47.3319 - 0.516 E) MeV

W_S = (5.716 + 0.4294 E + 0.0114 E^2) MeV

W_V = (0.0) MeV

V_{so} = (6.75) MeV

r_R = (1.2628 - 0.0039 E) fm

r_s = (1.3182 - 0.0039 E) fm

$r_{so} = r_R$

a_R = (0.7729 - 0.0058 E) fm

a_s = (0.4649 - 0.0035 E) fm

$a_{so} = a_R$

B. Reaction Cross Sections

The various compound nucleus reaction cross sections ($\sigma_{nn'}$, $\sigma_{n\gamma}$, σ_{CE}) were analyzed using the COMNUC Code.[45] This code provides a unified model of the compound nucleus reactions, thus assuring a consistent calculation. It embodies the rigorous theory of Moldauer[49,50] and includes a modification introduced by Tomita.[51] In addition it allows one to use a discrete level inelastic model as well as a continuum model so as to simultaneously handle these competitive processes in a coherent manner.

From Moldauer[49,50] the reaction cross section for incident channel c and outgoing channel c' ($c \equiv n\ell j$) may be written as:

$$\langle\sigma_{cc'}\rangle = \pi\lambda_c^2 \left[\frac{\langle\theta_{\lambda c}\rangle\langle\theta_{\lambda c'}\rangle}{\langle\theta_\lambda\rangle} W_{cc'} - \frac{\delta_{cc'}}{4} Q_c \langle\theta_{\lambda c}\rangle^2 \right] \quad (3)$$

$$\theta_\lambda = \sum_\alpha \langle\theta_{\lambda\alpha}\rangle \qquad \alpha \equiv \text{all open channels.}$$

$$W_{cc'} = \left\langle \frac{\theta_{\lambda c}\theta_{\lambda c'}}{\theta_\lambda} \right\rangle \Big/ \frac{\langle\theta_{\lambda c}\rangle\langle\theta_{\lambda c'}\rangle}{\langle\theta_\lambda\rangle} \quad (4)$$

where $W_{cc'}$ is the correction factor due to the width-fluctuation effect and

$$\langle\theta_{\lambda_c}\rangle = T_c + \frac{Q_c}{4}\langle\theta_{\lambda c}\rangle^2 \quad (5)$$

For Q_c small, the above relation becomes

$$\langle\sigma_{cc'}\rangle = \pi\lambda_c^2 \left[\frac{\langle\theta_{\lambda c}\rangle\langle\theta_{\lambda c'}\rangle}{\langle\theta_\lambda\rangle} W_{cc'} \right] \quad (6)$$

and $\langle\theta_\lambda\rangle = T_c$

T_c is the optical model transmission coefficient for channel c, and Q_c is the statistical parameter with range $o \leq Q_c \leq 2$.

Defining

$$\langle\theta_{\lambda c}\rangle = \frac{2}{Q_c}\left[1 - (1-Q_c T_c)^{1/2}\right] \tag{7}$$

Equation 5 becomes

$$\langle\theta_{\lambda c}\rangle = T_c + \frac{1}{Q_c}\left[1 - (1-Q_c T_c)^{1/2}\right]^2 \tag{8}$$

Thus in order that $\langle\theta_{\lambda c}\rangle$ be real the product $Q_c T_c$ should always be less than one. The parameter Q_c is defined by

$$Q_c = \frac{2B}{N^2}\left[1 - \phi_o\left(\frac{\langle\theta_{\lambda c}\rangle}{2N^2}\right)\right] \tag{9}$$

and

$$\phi_o(x) = 1 - \frac{1}{x}\left[1 - \frac{1}{x}e^{-x}\sin hx\right] - \frac{1}{x}\,Ei(-x). \left[\cos hx - \frac{\sin hx}{x}\right] \tag{10}$$

where the various quantities in equations 9 and 10 are the same as those defined by Moldauer.[49]

The parameters B and N have limited ranges of magnitude, namely $1 \geq B \geq 0$ and $N \geq 1$. In the limit, as

$$\frac{\Gamma}{D} \rightarrow 0, \quad B = 1, \; N = 1$$

$$\frac{\Gamma}{D} \rightarrow, \infty \quad B = 0, \; N = \infty.$$

In previous calculations the quantity Q_c was treated as a constant where its dependence on $<\theta_{\lambda c}>$ was ignored. However, as was discovered in several instances and also reported by,[52] such a treatment can lead to negative values for the compound elastic cross section for some partial waves when many channels are open and Q_c is not taken sufficiently small.

Following Tomita[51] this difficulty can be avoided if equation 5 is solved for $<\theta_{\lambda c}>$ by considering the functional dependence of Q_c on $<\theta_{\lambda c}>$ as given by equation 9.

The largest possible value for Q_c is given by B = 1 and N = 1.

The neutron capture cross section was defined in terms of the emission of dipole radiation in the compound nucleus given by

$$<\theta_{\lambda\gamma}> = 2\pi \left\langle \frac{\Gamma_\gamma}{D} \right\rangle_0 \rho(A,J,E),$$

where ρ is the density of levels at excitation energy E.

At energies greater than 14.0 MeV the capture cross section was assumed to be predominantly due to direct and collective effects and was analyzed in terms of FISPRO II[46] which is based on the theories of Lane and Lynn[53] and Brown.[54]

For the calculation of n-2n and n-particle cross sections such as $\sigma_{n,p}$; $\sigma_{n,d}$; $\sigma_{n,t}$; $\sigma_{n,\alpha}$ etc. the computer code THRESH[47] was used. This code is an empirical model code embodying the evaporation theory of Weisskopf. It is assumed that the high energy non-elastic cross-section is identifiable and that the competition for charged particle and neutron emission is a rather smooth function of the neutron-proton excess in the target-nucleus.

V. Calculations and Comparison with Experiment

A. A Resonance Region

1. Total Cross Section

For neutron energies less than 650 keV the data files of ENDF/III were used directly. These data are based on the experimental results reported by Stieglitz et al.[8] and Bowman et al.[5]

Figures 5 and 6 show a comparison of a single level Breit-Wigner fit (using code RESEND) with experimental data for natural chromium. (This fit has not been Doppler broadened.)

In determining the total widths Γ_T, for energy $E \geq 575$ keV it was assumed that the inelastic width Γ_n, due to the 564 keV level in ^{53}Cr was negligible and was set equal to zero up to 700 keV. No complication arose due to this assumption since the inelastic scattering cross section also is zero for $E < 700$ keV.

2. Radiative Capture Cross Section

For neutron energies less than 650 keV the data files of ENDF/III were used, employing the same experimental results as

reported from the calculation of σ_{Tot} in the resonance region. Average radiation widths were assigned for the isotope, where data was lacking.

Le Rigoleur et al.[55] have reported absolute capture measurements between 70 to 550 keV.

Between 90 keV and 160 keV their values are somewhat higher than most experiments, however the average cross sections are in rather good agreement with Stieglitz et al.[8] as can be seen in Table 6.

For energies between 200 and 600 keV Le Rigoleur et al.[55] reports better agreement with other experimental data (see BNL 325, second edition).

3. Elastic Scattering Cross Section E < 650 keV

The cross section for elastic scattering may be described by the same methods outlined for σ_T and $\sigma_{n\gamma}$ in the resonance region.

Since the radiation widths are so much smaller than the neutron widths the elastic cross section is practically identical to the total cross section. Therefore only the total cross sections as seen in Figures 5 and 6 are given.

For the angular distributions of the elastically scattered neutrons the experimental data of Smith[56] and Elwyn[57] were used along with optical model calculations, thereby yielding sufficient material to describe the angular distributions of the secondary neutrons in File 4 of ENDF.

B. High Energy Cross Sections

1. Total Cross Sections

The amount of experimental data on the total cross section at high energies for natural chromium is voluminous, with the various references too numerous to be mentioned here. (Some of these were mentioned in Section III.) The reader is referred to the CSISRS listing or CINDA for other references.

For the purpose of this evaluation the most recent data of Perey et al.[13] was used. Perey and his co-workers have carried out time of flight measurements on natural chromium for 0.18 to 30 MeV.

For the Cr evaluation this data was fitted using a spline fitting technique and the total cross sections are shown in figures 7 to 16.

As can be seen up to an energy of about 3.9 MeV the total cross section has a well defined structure which allowed a rather succinct interpretation of the cross section using a spline fit. Beyond this energy the cross sections become less defined with the spline fitting procedure yielding an average value through the dispersive data points.

Table 11 presents a comparison with the total cross sections assumed by Holmqvist and Wiedling[16] and Kinney and Perey[17] in their analyses. Also given is the spline fit interpretation which was used in the evaluation and the Optical Model results at the same energy points. The difference between these latter two descriptions is less than 1.5%, and as seen from

figures 15 and 16 either the spline fit or model calculation would provide adequate description of the total cross section.

2. Radiative Capture Cross Section

Above the resolved energy region ($E \gtrsim 0.7$ MeV) the capture cross sections were determined from calculations using COMNUC[45] for the compound nucleus capture taking into account $\sigma_{nn'}$ competition and FISPRO[46] for the direct and collective capture. At energies greater than 10 MeV the capture cross section resulting from compound nuclear processes was negligible and the calculated direct and collective results were normalized to the 14 MeV experimental point of CVELBAR et al.[18]

This direct and collective calculation resulted in a slight peaking of the cross section at E_n = 17 MeV as seen in Figure 17. A similar peak at about the same energy was reported by Nishimura et al.;[58] however, their results are high by about a factor of two. This could probably be due to the fact that they did not normalize to the 14 MeV data point of Cvelbar.[18]

3. Non-Elastic Cross Section

The non-elastic cross section, up to about 5.0 MeV, is due primarily to $\sigma_{nn'}$ and $\sigma_{n\gamma}$.

Slightly above this energy, the n,p and n,α contributions become significant. At still higher energies, the n,2n and other reactions must be considered.

Direct measurements of σ_{non} are practically nil. There is a rather old set of experimental data by Taylor et al.[59] who carried out spherical shell transmission measurements in the

energy range of 3.5 to 14.1 MeV. There is one other experimental measurement at E = 2.5 MeV (σ_{non} = 1.4 ± 0.3b) reported by Pasechnick[60] and Strizhak.[61]

Up to E = 4.0 MeV, the non-elastic cross section was determined from the experimental data on $\sigma_{nn'}$ and $\sigma_{n\gamma}$, with σ_{non} = $\sigma_{n\gamma}$ for E < 650 keV.

In evaluating σ_{non} for the higher energies a combination of the experimental direct measurements of Taylor et al.[59] and the σ_{Tot} and σ_{el} measurements of Kinney and Perey[17] were used in conjunction with the optical model calculations.

A comparison of the evaluated, experimental and model calculations are shown in Figure 18. In this figure σ_{non} is not zero at 650 keV as depicted but 3.8 mb which is too small to be seen on the linear-linear plot.

4. Elastic Cross Section

For energies less than 1.5 MeV and above the resonance region quite a few measurements have been made for the differential and total elastic scattering cross section. A. B. Smith[56] has carried out experiments for incident energies of 0.3 to 1.5 MeV.

Other measurements in this range have been reported by Cox[62] for energies 0.7 to 1.2 MeV and Elwyn et al.[57] in the energy 0.35 to 0.96.

This data was used primarily for describing the angular distributions of the secondary neutrons (File 4).

The total elastic cross section was taken to be the difference between the total and non-elastic cross section. Thus the high degree of structure that is evident in the total cross section manifests itself in the elastic, as can be seen in Figures 19 to 26.

The angle integrated data of Smith[56] is compared with the evaluated elastic cross sections in Figures 19 to 22. (The experimental errors have been suppressed so as to alleviate graphic congestion.)

Additional angular distributions necessary to fill the gaps where experimental data were lacking were described by Optical Model calculations.

For energies greater than 1.5 MeV the amount of experimental elastic scattering data is rather sparse, with the major portion being provided by Holmqvist[63] and Holmqvist and Wiedling[16,64] (figures 23 to 28) and the more recent results of Kinney and Perey[17] (5 pts. for E = 4.34 to 8.56 MeV) Figures 26 and 27.

For E > 5.0 MeV the data of Holmqvist and Wiedling is consistently smaller than that of Kinney and Perey. This is felt to be due to the fact that in the analytical fits to the angular distribution, the data of Holmqvist and Wiedling failed to satisfy the Wick limit (see Reference 63, Table 17).

$$\frac{d\sigma(0°)}{d\Omega} \geq \left(\frac{k}{4\pi}\sigma_T\right)^2$$

This violation causes the total elastic cross section to be about 10% too low. This discrepancy has also been pointed out by Kinney and Perey[17] and Slavik (KAPL-priv. commn.).

Beyond these two sets of experimental data (E > 8.56 MeV) only one angular distribution for elastic scattering exists; namely at 14.0 MeV by Stelson et al.[65] Thus it was necessary to fill in the gaps and extend the range to 20.0 MeV (see Figures 27 and 28) by carrying out Optical Model Calculations.

The comparison of these model calculations with the angular experimental data is shown in Figures 29 to 39 along with the Wick limit.

A tabular comparison of the angular integrated values is given in Table 11 along with the total cross sections.

Table 11 shows that the spline fit to σ_T of the ORNL data for E > 5.0 MeV is practically identical to the σ_T assumed by Kinney and Perey.[17] Thus the resulting elastic cross sections are in excellent agreement with each other. The σ_T values quoted by Holmqvist and Wiedling[16,64] differ only slightly from the ORNL/BNL values but this is probably because they are using a different set of experimental data - Foster and Glasgow.[14]

Of most significance is the fact that the Optical Model calculations and the evaluated σ_{el} are in agreement (within experimental error) with the angle integrated data of ORNL. It is also evident that the angle integrated values of Holmqvist and Wiedling are about 10% lower than that of ORNL and BNL (see Figures 26 and 27).

This agreement between the Optical Model calculations of the differential scattering and the experimental data (Figures 29 to 39) provided adequate confidence in using the calculated results of the differential elastic scattering for generating the Legendre coefficients in File 4 over a much finer mesh than that permitted by the sparsity of experimental data.

5. Inelastic Cross Sections

Quite a bit of effort went into evaluating the inelastic cross section for natural chromium, since this reaction is deemed most important in fast reactor analyses.

Model calculations based on the Hauser-Feshbach formulism with Moldauer fluctuation corrections provided a statistical treatment for both the discrete and continuum inelastic cross sections for $^{50,52,53,54}Cr$. In addition, due to its high abundance, coupled-channel calculations were carried out for ^{52}Cr for the description of the direct inelastic components.

The energy level scheme for the chromium isotopes are shown in Tables 7 to 10.

The low lying levels in ^{52}Cr were assumed to be vibrational, thus collective inelastic excitations were calculated assuming $0\text{-}2^+$; $0\text{-}2^+\text{-}3^-$; and $0\text{-}2^+\text{-}4^+$ coupling.

The higher states are weakly coupled to the ground state so their contributions to the direct inelastic excitations were taken to be negligible.

5a. Comparison of Calculations with Experimental Data for Cr Isotopes

For energies up to 3.3 MeV the most extensive experi-

mental investigation of the total inelastic neutron cross sections for natural Cr and each of its four stable isotopes has been carried out by Van Patter et al.[29]

Differential gamma-ray spectra from the (n,n'γ) reaction were analyzed and converted to inelastic neutron cross sections in these experiments.

They also reported results for the discrete excitations of the low lying levels in ^{52}Cr and ^{53}Cr.

Corrections for anisotropic angular distributions in ^{52}Cr about $\theta = 100°$ were made by Van Patter et al for the following levels [MeV(Jπ)]

1.434 (2+); 2.37 (4+); 2.768 (4+); 2.965 (2+);
3.162 (2+).

(They did not observe any excitation of the 3.114 (6+).) In their measurements on ^{53}Cr no corrections for anisotropy were made, thus the following level excitations cross sections were assumed to be isotropic;

0.564 ($1/2^-$); 1.01 ($5/2^-$); 1.29 ($7/2^-$); 1.98 ($7/2^-$);
2.33 ($3/2^-$).

D. L. Broder[30] et al have also carried out measurements on ^{52}Cr up to 3.0 MeV, likewise using gamma-ray production cross sections determined from the de-excitation of the excited states.

Similar type measurements on ^{52}Cr have also been reported by Degtyarev and Protopopov[32,66] for energies between 1.8 and 3.8 MeV.

Abramov[33] and Glazkov[34] carried out inelastic scattering on Cr and ^{53}Cr respectively by measuring the neutron pulse spectra with and without a scatterer using inverse spherical geometry.

Kinney and Perey[17] have recently measured the inelastic cross sections for natural Cr between 4.07 and 8.56 MeV and for ^{52}Cr for energies between 6.44 and 8.56 using time-of-flight techniques.

In order to obtain meaningful comparisons of the theoretical calculations with experiment, certain corrections had to be considered. First the calculations for the inelastic cross sections for the individual isotopes, when weighted by their respective abundances, had to be renormalized so as to be in agreement with the total inelastic cross section of natural Cr, which in turn had to be made consistent with the predictions in the non-elastic,

i.e. $\sigma_{nn'}(Tot) = \sigma_{non} - (\sigma_{n,\gamma} + \sigma_{n,2n} + \sigma_{n,3n} + \Sigma\sigma_{nx} + \Sigma\sigma_{nxn'} + \Sigma\sigma_{nn'x})$

where x = p, t, d, He^3, He^4.

Also, the inconsistency between the Hauser-Feshbach calculations of the inelastic scattering and the coupled-channel calculations was removed by introducing a reduction factor R given by

$$R = \frac{\sigma_{expt'l} - \sigma_{DI}}{\sigma_{expt'l}}$$

where it has been assumed that the difference between the experimental inelastic cross section and the direct inelastic cross section is the true compound inelastic cross section.

The results of such interpretation between experiment and calculations are shown in Figures 40 to 52.

The experimental (n,n') cross sections for some low lying states in ^{52}Cr and ^{53}Cr are shown in Figures 40 to 48. Also shown are the comparisons with the evaluated (n,n') cross sections based on the statistical model and direct interaction analysis.

In Figure 40, the first 2+ level of ^{52}Cr at 1.434 MeV shows a wide dispersion in the experimental data in the energy region 1.5 to 3.5 MeV which is possibly due to the structure that exists in the inelastic excitations around these energies.

The data points on Figures 40 and 41 for natural chromium reported by Kinney and Perey[17] have been weighted by the inverse abundance of ^{52}Cr for comparison purposes. This ORNL data, along with the ^{52}Cr points at 6.44, 7.54 and 8.56 MeV, furnished sufficient information to define the excitation cross section at the higher energies.

The only experimental data for the ^{53}Cr low lying excitations is that of Van Patter et al.[29] The evaluated curves that were used for determining their contribution to natural Cr are shown in Figures 46 to 48, along with the measurements of Van Patter et al.[29]

For the calculation of the total inelastic of each chromium isotope, the level schemes of Tables 7 to 10 were employed.

The analysis was carried out for energies up to 20.0 MeV and included the discrete as well as the continuum. Of course it was necessary to renormalize the calculations so as to take into consideration the competition of $\sigma_{n\gamma}$ (which was negligible) and the (n,2n), (n,3n) and (n-particle) reactions.

The low energy cut-off for the continuum for each isotope was

^{50}Cr E_c = 1.9 MeV

^{52}Cr E_c = 3.8 MeV

^{53}Cr E_c = 1.6 MeV

^{54}Cr E_c = 1.9 MeV

These cut-off energies are somewhat arbitrary but are necessary so as to attenuate the magnitude of the calculated discrete excitation due to possible missed (experimentally undefined) levels.

In ^{50}Cr (Figure 49) the main contribution to the total inelastic cross section (up to about 3.0 MeV) is seen to come from the 0.783 level. Similarly in ^{54}Cr the main contributor is the first 2+ level at 0.8348 MeV (see Figure 52).

In ^{53}Cr the second excited state 1.006 ($5/2^-$) is about a factor of two higher than the first excitated state 0.564 ($1/2^-$) which offers about the same contribution as the third excited state 1.287 ($7/2^-$).

Van Patter et al did not see any excitations of the 1.539 ($7/2^-$), 2.173 ($11/2^-$), 2.233 ($9/2^-$) levels. However, the calculated values of their experimentally resolved levels in ^{53}Cr (Figures 44 to 48) added together (Figure 51) somewhat underestimates the total inelastic cross-section. Adding the missed levels, however, somewhat overestimates the total inelastic (Figure 51), nonetheless it is felt that these levels should be taken into consideration. The excellent agreement of the evaluated with the total experimental inelastic data of Van Patter et al.[29] and that of Broder et al.[30] for the major isotope (^{52}Cr) is seen in Figure 50.

5b. Differential Inelastic Scattering

Figures 53 to 58 show the comparison between the compound differential inelastic and the direct differential inelastic and the direct differential inelastic (coupled-channel calc.) of the 1.434 (2+) and 2.369 (4+) levels in ^{52}Cr. The sum of the compound and direct contribution produces the total differential inelastic cross section. The experimental data is that of Kinney and Perey.[17] Note the symmetry about 90° in the compound inelastic process (Hauser-Feshbach calc.) as compared to the high forward peaking in the direct process.

This forward peaking accounts for some asymmetry about 90° in the calculations as is to be expected, although the Kinney and Perey[17] data does not show this since their measurements ranged only from 35.7 to 135.4 degrees.

The measurements at 14.6 MeV[65] shown in Figure 60 definitely shows the high degree of anisotropy in the differential inelastic which is assumed to be due primarily to the direct excitation of these levels. The coupled-channel calculations while producing a satisfactory shape slightly underestimated the magnitude of the cross section by about 20%. However, it should be mentioned that this experimental data of Stelson et al.[65] are for natural Cr which means that the low lying level possibly contains a contribution from the 1.3 ($7/2^-$) MeV level in ^{53}Cr. The solid curves in Figure 59 have been normalized to the experimental data at 60°.

5c. Inelastic Cross Sections for Natural Cr

The foregoing analysis of the isotopic Cr inelastic cross sections was abundance weighted to provide the inelastic contributions for natural Cr.

These results are presented in Figures 60 to 100 for the various discrete level excitations for natural Cr. While all the levels shown in Table 7 to 10 were used in calculating the excitation functions for the various isotopes, only the first low lying levels of ^{50}Cr (0.7831 MeV) and ^{54}Cr (0.8348 MeV) were put into ENDF/B as discrete. The rest of the level excitations for these two isotopes were put into the continuum. This was necessary since the present ENDF format allows for only 40 discrete levels.

On the other hand, all the levels for ^{52}Cr except the last at 7.900 MeV, and all those for ^{53}Cr were taken into consid-

eration, giving a total of 23 and 15 excitations in the discrete region for ^{52}Cr and ^{53}Cr respectively.

The most important level due to its large contribution is the 1.434 MeV level of ^{52}Cr. The amount of experimental data for this level provided adequate confirmation for both its magnitude and shape (see Figures 40 and 65). Similar comments may be made about the 2.369 MeV level of ^{52}Cr (Figures 41 and 71). In Figure 77 the data of Van Patter has been reduced by the isotopic abundance of ^{52}Cr so as to establish the magnitude of this excitation (2.965 MeV) for natural Cr. The data points reported by Kinney and Perey[17] shown on this figure were determined from only three measurements of angular distribution ranging from about 70 degrees to 87 degrees for E = 4.65 and 5.23 MeV incident neutron energies and from 49 to 64 degrees for the 5.5 MeV point. Kinney and Perey then assumed an average $\frac{d\sigma}{d\Omega}$ along with an isotropic distribution. This leads to a rather wide dispersion in the data as can be seen in Figure 77. The calculated inelastic cross section for this level was normalized to the data of Van Patter et al.,[29] leading to the evaluated curve shown in the figures which agrees with the 4.65 MeV point of Kinney and Perey[17] and falls between their other two measurements.

Scattering to the continuum in natural chromium is shown in Figure 101 and includes the contributions of all four isotopes.

The total inelastic scattering for natural chromium is shown in Figures 102 and 103 from threshold to 20.0 MeV.

The evaluated curve includes the abundance weighted discrete and continuum, contributions of all four isotopes.

As can be seen in Figure 102, the experimental data on the total inelastic cross section shows structure which could be real, reflecting the structure that is seen in the total cross section in this energy range.

Another possible cause for the wide dispersion might be attributed to the different experimental techniques employed.

The wide gap in the experimental data for $E_n > 3.5$ MeV necessitated that careful consideration be given to the competing processes (n,2n), (n,3n), (n,particle) in order that an adequate interpretation of the total inelastic cross section would result in the high energy region. The various experimental results around 14.0 MeV were of particular importance in satisfying this criteria.

Having established rather good agreement between the optical model calculations and the experimental results of Taylor et al.[59] for the non-elastic cross sections; the contributions for all competing processes were subtracted such that

$$\sigma_{nn'} = \sigma_{non} - (\sigma_{n,2n} + \sigma_{n,3n} + \sigma_{n\gamma} + \Sigma\sigma_{nn'x} + \Sigma\sigma_{nxn'})$$

The results of this procedure are shown in Figure 104 where the agreement between the experimental and evaluated values is rather good.

A few details of these experimental points at 14 MeV are worth mentioning since their interpretation played a very

succinct role in fixing the value of the cross section at this energy.

Salnikov and Lovchikova[67] analyzed the energy spectra of the inelastically scattered neutrons at various angles and thus obtained the differential inelastic cross section.

They reported a value of $\sigma_{nn'}$ = 880 ± 40 mb.

Fujita et al.[36] also measured the continuous spectra of inelastically scattered neutrons using a time-of-flight method.

They made their measurement at only one angle (θ = 110°) and assumed isotropic scattering. Their value of $\sigma_{nn'}$ = 1.27 ± 0.126 b was not used in the evaluation since it is at great variance with other measurements at this energy.

The probable reason for this high value is due to the fact that they assumed isotropic scattering and ignored certain n-particle reactions.

Tageson and Hille[68] along with Breunlich and Stengel[69] detected the gamma-rays resulting from the deexcitation of the excited states similar to the method of Van Patter et al.[29] Tageson and Hille[68] established an upper bound of $\sigma_{nn'}$ = 870 ± 70 mb based on certain observations of the n-2n reaction. They also carried out an absolute determination of the inelastic cross section achieving a value of $\sigma_{nn'}$ = 740 mb ± 20% reported by Morgan et al.[701]

Breunlich and Stengel[69] quote a value of $\sigma_{nn'}$ = 790 ± 112 mb of which, based on an assumption by Uhl[71] that 100 mb is due to the direct inelastic scattering process.

Colli and Marcazzan[72] have also reported that at 14 MeV pre-compound emission might account for as much as 30% of the inelastic cross section.

The combined results of the (n,2n) and (n,particle) cross sections were determined to be 0.50 b at 14.0 MeV (see next section). From a value of σ_{non} = 1.30b, the total inelastic scattering cross sections turns out to be 0.8 b which is in excellent agreement with the aforementioned experimental results.

This agreement at 14.0 MeV provides a rather high level of confidence for the total inelastic scattering in the energy region 3.5 to 20.0 MeV.

6. n,2n Cross Section

No experimental data exists for the n,2n reaction of natural chromium, thus one has to rely rather heavily on model code interpretation.

The results of THRESH were combined with the experimental data of References 19, 23, 24, 26, 27, 73 to 78 on ^{50}Cr and ^{52}Cr, with a normalization chosen so as to reproduce the fast rising cross section just above threshold which is deemed the most important region.

Figures 104 and 105 depict the evaluated $\sigma_{n,2n}$ for ^{50}Cr and ^{52}Cr. The data of Qaim[76] at 14.7 MeV was used for normalizing the ^{50}Cr calculations. This yielded very good results up to about 17 MeV, deviating somewhat from the Bormann[24] conclusion by about 25 mb. Due to its low abundance, this non-agreement is not expected to seriously affect the n,2n reaction for natural Cr.

A most recent experimental value of $\sigma_{n,2n}$ = 24 ± 5 mb at 14.7 MeV has been reported by Holmberg et al.[79] For ^{52}Cr the 14.0 MeV experimental value of Kenna and Harrison[19] was used for normalization which also reproduced good agreement up to about 16.0 MeV with the work of Bormann et al.[23] Beyond 16 MeV the model calculations overpredicted the Bormann[23] results (note this is the opposite of the ^{50}Cr analysis) by about 20%.

The reported estimates[19] for the experimental (n,2n) cross section of ^{53}Cr ($\sigma_{n,2n}$ = 861 mb at 14 MeV) and ^{54}Cr ($\sigma_{n,2n}$ = 794.0 mb at 14 MeV) were used to normalize the THRESH calculation for these isotopes.

Combining these results with those of ^{50}Cr and ^{52}Cr led to an evaluated (n,2n) cross section for natural Cr as indicated in Figure 106.

7. N,Particle Cross Sections

The amount of experimental data on the n,particle reaction cross sections for the various isotopes of Cr is very sparse and again the model calculations of THRESH were used to predict these various reactions.

a. (n,p) Cross Section

The evaluated results for the (n,p) cross sections in ^{53}Cr and ^{52}Cr are shown in Figures 107 and 108. As can be seen in Figure 107 for ^{53}Cr (n,p) the experimental data points are all clustered about 14.0 MeV so the model parameters were chosen so as to have agreement with the most recent data of Kenna and Harrison[19] and also that of Prasad and Sarker.[80]

After this evaluation was completed two recent measurements for the (n,p) cross section for ^{53}Cr were reported. Levkovskii[81] measured a value of σ_{np} = 44 ± 10 mb at E = 14.0 MeV and Holmberg et al.[82] reported a value σ_{np} = 40 ± 7 mb (E = 14.7 MeV).

As can be seen from Figure 107 the evaluated (n,p) cross section is in good agreement with these recent measurements.

In ^{52}Cr there is also quite a bit of data around 14 MeV, along with one reported measurement by Wilhelmi[83] around 8 MeV which served to describe the rapid increase of σ_{np} above 5.0 MeV (see Figure 108).

Kern et al.[20] have carried out a rather extensive set of measurements for ^{52}Cr (n,p) V^{52} using the activation method where the gamma rays following β decay were counted.

As seen in Figure 108 the (n,p) cross section of Kern et al.[20] decreases from about 125 mb at 12 MeV to about 70 mb at 18 MeV.

The more recent measurements of Kenna and Harrison[19] and Prasad and Sarkar[80] around 14 MeV are approximately about 50% smaller than those of Kern et al.[20] Thus the model calculations were normalized (in this energy region) to this 14.0 MeV data of Kenna and Harrison[19] which gives good agreement with other individual measurements[84-91] on ^{52}Cr.

The evaluated (n,p) cross section is consistent with the calculations of Savel'ev et al.[92] and the early empirical and systematic treatment of Levkovskii[90] and with the most

recent experimental values reported by Levkovskii[81] and Holmberg et al.[82] For the two remaining isotopes, the data is very sparse. For ^{50}Cr the data of Kenna and Harrison[19] and D. L. Allan[94] was used.

For ^{54}Cr the value reported by Husain and Kuradon[88] at E = 14.8 (σ_{np} = 13.5 ± 1.5 mb) was used for normalization of the model calculations. This is in good agreement with the recently measured value of σ_{np} = 15 ± 4 mb at E = 14.7 MeV.[82].

The individual evaluated (n,p) cross sections for the four isotopes were then abundance weighted to yield the evaluated (n,p) reaction cross section for Cr (nat) as shown in Figure 109.

b. (n,He4) Cross Sections

Dolya et al.[91] at the 1973 Kiev conference reported on their direct measurement at 14.7 MeV of the (n,α) cross section for all four chromium isotopes. These were angular distribution experiments ranging from 0 to 150 degrees, whose integrated cross sections produced the following:

^{50}Cr ($\sigma_{n\alpha}$ = 121.0 ± 8.5 mb)

^{52}Cr ($\sigma_{n\alpha}$ = 40.2 ± 3.6 mb)

^{53}Cr ($\sigma_{n\alpha}$ = 45.1 ± 3.7 mb)

^{54}Cr ($\sigma_{n\alpha}$ = 37.2 ± 3.0 mb)

The evaluated $\sigma_{n\alpha}$ for ^{53}Cr and ^{52}Cr are shown in Figures 107 and 108. The σ (n,He4) values for the natural element is seen on Figure 110.

c. Other n,particle Reactions

The amount of experimental data on reactions such as (n,t), (n,d), (n,np) etc. is very very meager and the evaluation is highly model dependent. However, due to the high threshold for these reactions (see Tables 2 to 5) they are expected to be of the order of a few milli-barns even at 20.0 MeV.

Figures 111 to 115 present the evaluated reaction cross sections for the (n,d), (n,t), (n,np), (n,He-3) and (n,n He-4) reactions.

In Figure 113 the sum of $\sigma_{n,np}$ and $\sigma_{n,pn}$ is given and in Figure 115 the combination for $\sigma_{n,n\alpha}$ and $\sigma_{n,\alpha n}$ is shown.

The other reaction cross sections e.g. n,3n etc. have thresholds > 20 MeV or are so high that their contributions are negligible.

VI. Gamma Ray Production Cross Sections

At the time of this writing there have been no measurements of the total gamma production cross sections ($\sigma_{n,x\gamma}$) for Cr. There have been some discrete measurements for the (n,n'γ) reactions (e.g. Kichen and Goodin) and a little data exists for gamma rays from neutron capture.

Due to this crucial lack of experimental data it was necessary to carry out the analysis using an empirical calculation formalism.*

*The evaluation for the photon production data for Cr was carried out by R. J. Howerton et al (LLL) (private communication).

This approach is based on the method reported by Howerton and Plechety[95] and recently modified by Perkins,[96] so as to include more detailed information of the energetics of the neutron induced reactions and to consider the competition of internal conversion.

The capture gamma ray spectrum for both discrete levels and the continuum was taken from the experimental data of Orphan et al.[97]

The composite (n,xγ) cross sections were lumped together with the line data taken from the literature and the continuum based on the extended formalism of Perkins et al.[96]

The error estimates range from 20% to 30%.

VII. Conclusions and Recommendations

In an attempt to carry out as complete an evaluation as possible on Cr, it has been necessary to combine the results of experiment with the most sophisticated nuclear models and empirical formalisms available.

Tables 2 to 5 show that the thresholds for many n,particle reactions lie well below 20 MeV, and Figures 1 to 4 indicate that much more experimental data is required on the various isotopes of Cr.

Nonetheless, the evaluation contained herein is felt to embody all the necessary features pertinent to the analysis of fast reactors.

The associated error estimates for the various reactions in the evaluation are given in Table 12.

Acknowledgement

The author would like to express his appreciation to the various members of NNCSC who rendered assistance in this evaluation. In particular the diligent participation of Jerry Holm and Bob Kinsey of NNCSC, who performed the spline-fits to the experimental total cross section and who aided in putting the files together, is gratefully acknowledged.

An expression of gratitude is also extended to W. E. Kinney and F. G. Perey of ORNL who provided their experimental data prior to publication.

In addition a word of thanks is in order to Bob Howerton (LLL) who carried out the photon production evaluation.

REFERENCES

1. N. Azziz et al, WCAP 7281 (1969).
2. BNL 325 - Third Edition, Vol. 1 (1973).
3. E. G. Bilpuch et al, Ann. Phys 14 (1961) 387.
4. J. A. Farrel et al, Ann. Phys 37 (1966) 367.
5. C. D. Bowman et al, Ann. Phys. 17, 319 (1962).
6. H. Beer et al, KFK 1517 (1972).
7. K. N. Muller and G. Rohr, KFK 1230 (1970).
8. Stieglitz et al, Nucl. Phys. A163 (1971) 592.
9. A. Bratenahl et al, Phys. Rev. 110, 927 (1958).
10. F. Manero and M. A. Vignon, Nucl. Phys. A 119, 356 (1968).
11. S. Cierjacks et al, KFK 1000 and Suppl. (1968).
12. L. Green and J. A. Mitchell, WAPD-TM-1073 (1973).
13. F. G. Perey and W. E. Kinney (Priv. Comm.) (1973) (See CSISRS).
14. D. G. Foster and D. W. Glasgow, Phys. Rev. C3, 576 (1971).
15. Oyumin et al, Bull. Acad. Sci USSR 36 (4), 771 (1972).
16. B. Holmqvist and T. Wiedling, AE-430 (1971).
17. W. E. Kinney and F. G. Perey, ORNL-4806 (1974).
18. F. Cvelbar et al, Nucl. Phys. A130, 401 (1969).
19. B. T. Kenna and P. E. Harrison, SLA-73-0637 (1973).
20. B. D. Kern et al, Nucl. Phys. 10, 226 (1959).
21. L. Husain, Jour. Inorg. and Nucl. Chem. 29, 2665 (1967).
22. G. P. Dolya et al, Kiev Conf. 1973
23. M. Bormann et al, Nucl. Phys. A115, 309 (1968).
24. M. Bormann, CSISRS (unpublished) (1965).
25. S. M. Qaim, Nucl. Phys. A185, 614 (1972).

26. S. M. Qaim et al, Proc. Int'l. Conf. Canterbury (1971).

27. Boedy, Budapest Conf. (1972).

28. S. M. Qaim and Stocklin, J. Inorg. Nucl. Chem. 35, 19 (1973).

29. D. M. Van Patter et al, Phys. Rev. 128, 1246 (1962).

30. D. L. Broder et al, Sav. J. At. En. 16, 113 (1965).

31. R. M. Kiehn and C. Goodman, Phys. Rev. 95, 989 (1954).

32. Yu G. Degtyarev and V. N. Protopopov, J. At. En. 23, 1350 (1967).

33. A. I. Abramov, Sav. J. At. En. 12, 65 (1962).

34. N. P. Glazkov, Sov. J. At. En. 15, 416 (1963).

35. Transl. by D. L. Allen, J. Nuc. En. 18, 656 (1964).
Salinikov et al, BNL-TR-545 (1973).

36. I. Fujita et al, J. Nucl. Sci. and Tech. 9(5), 301 (1972).

37. G. Grenier (CEA), Reported at Kiev Conf. (1973).
J. Phys. 18(2), 263 (1973).

39. U. Abbondanno et al., J. Nucl. En. 27, 227 (1972).

40. R. E. Coles, AWRE O-41/71 (1971).

41. Von M. Wollensen, Atom Kernenergic 20 (3), 227 (1972).

42. Yu G. Degtyarev and V. N. Protopopov, Bull. Acad. Sci. USSR 35 (11) 2123 (1971).

43. ABACUS 2 - E. H. Auerbach BNL-6562 (unpublished).

44. JUPITOR 1 - T. Tamura ORNL-4152 (1967).

45. COMNUC., C. Dunford, AI-AEC-12931.

46. FISPRO., V. Benzi, et al, CEC (69) 24.

47. THRESH., S. Pearlstein, J. Nucl. En. 27, 81 (1973).

48. T. Tamura, Rev. Mod. Phys. 37, 679 (1965).

49. P. A. Moldauer, Phys. Rev. 135B, 642 (1962).

50. P. A. Moldauer, Rev. Mod. Phys. 36, 1079 (1964).

51. Y. Tomita, Japan At. En. Res. Inst. Rpt JAERI-1191 (1970).

52. K. Tsukada et al, Nucl. Phys. A125, 641 (1969).

53. A. M. Lane and J. E. Lynn, Geneva Conf. 1958 (Vol. 15, p. 38).

54. G. E. Brown, Nucl. Phys. 57, 339 (1964).

55. Le Rigoleur et al, 1973 (unpublished).

56. A. B. Smith, 1066 (unpublished) see BNL 400, Third Edition (1970).

57. A. J. Elwyn et al, Bull. Am. Phys. Soc. 12, 473 (1967).

58. K. Nishimuva et al, Helsinki Conf. 1970, IAEH-CN-26/28.

59. H. L. Taylor et al, Phys. Rev. 100, 174 (1955).

60. M. V. Pasechnik, Geneva Conf. 1955, P/714.

61. V. I. Strizhak, JETP 4, 769 (1957) Eng. Transl.

62. S. A. Cox, B. Am. Phys. Soc. 10, 576 (1965).
Also see BNL 400 (Third Edition) (1970).

63. B. Holmqvist, Ark. Fys. 38, 403 (1968).

64. B. Holmqvist and T. Wiedling, AE 366 (1969).

65. P. H. Stelson et al, Nucl. Phys. 68, 97 (1965).

66. Yu G. Degtarev and V. N. Protopopov, Bull. Acad. Sci. USSR, Phys. Series 35 (11) 2123 (1971).

67. O. A. Salinikov and G. N. Lovchikova, Helsinki Conf. (1970) IAEA-CN-26/79 (BNL TR-545) (1974).

68. S. Tageson and P. Hille (1965), Translated from Mitteilun, des. Inst. für Kadium furschung., No. 574.

69. W. Breunlich and G. Stengel, Z. Naturforsch 26A, 451 (1971).

70. I. L. Morgan et al, TID 20658 (unpublished).

71. M. Uhl, Nucl. Phys. A184, 253 (1972).

72. L. M. Colli and G. M. Marcazzan, Riv. d. Nouro Cim. 3(4), 535 (1973).

73. L. A. Rayburn, Phys. Rev. 122, 168 (1961).

74. C. S. Khurana and H. S. Hans, Nucl. Phys. 28, 560 (1961).

75. S. K. Mukherjee et al, Proc. Phys. Soc (Lond) 77, 508 (1961).

76. S. M. Qaim, Nucl. Phys. A 185, 614 (1972). - Calculated

77. R. Wenusch and H. Vogach, Oesterr. Aked. Wiss., Math and Nehure W. Arzeiger 99, 1 (1962).

78. G. N. Maslov et al, Jadernye Konstanty 9, 50 (1972).

79. Holmberg et al, J. Inorg. Nucl. Chem. 36(4) 715 (1974).

80. R. Prasad and D. C. Sarkar, Nouvo. Cimuto 3A, 467 (1971).

81. W. N. Levkovskii, Sov. J. Nucl. Phys. 18(4), 361 (1974).

82. P. Holmberg et al, J. Inorg. Nucl. Chem. 36(4), 715 (1974).

83. F. Wilhelmi, Geneva Conf. Proc. Vol. 2 (1955).

84. C. S. Khurana and I. M. Gavil, Nucl. Phys. 69, 153 (1965).

85. D. M. Chittenden and D. C. Gardner, Ann. Prog. Rpt. Nucl. Chem. (1961) (Univ. of Arkansas) Unpublished.

86. E. B. Paul and R. L. Clarke, Can. J. Phys. 31, 267 (1953).

87. S. K. Mukherjee et al, Proc. Phys. Soc. 77, 508 (1961).

88. L. Husain, P. K. Kuradon, Jour. Inorg. and Nucl. Chem. 29, 2665 (1967).

89. B. Mitra and A. M. Ghose, Nucl. Phys. 83, 157 (1966).

90. V. N. Levkovskii, Sov. Phys., JETP 18, 213 (1964). - Calculated

91. G. P. Dolya et al, Kiev. Conf. (1973).

92. A. E. Savel'ev et al, Sov. J. Nucl. Phys. 15(4), 416 (1972).

93. S. M. Qaim, Inst. für Nuk., Kern furs. (Julich), Presented at 167th Nat'l. Meeting of the American Chemical Society, Los Angeles, Calif., March 1974.

94. D. L. Allan, Nucl. Phys. 24, 274 (1961).

95. R. J. Howerton and E. F. Plechety, Nucl. Sci. and Eng. 32, 178 (1968).

96. S. T. Perkins et al, UCRL 75640 (1974).

97. V. J. Orphan et al, GA-10248 (1970).

Table 1

Comparison of ENDF III and ENDF IV

Neutron Reactions	MF	MT	ENDF/III	ENDF/IV
σ_{tot}	3	1	Resonance region (E_c=650 keV) Smooth data 650 keV to 15.0 MeV	Resonance Region (E_c=642.85 keV) Smooth data 642.85 to 20.0 MeV
σ_{el}	3	2	Same as MT=1	Same as MT=1
σ_{non}	3	3	--	Same as MT=1
$\sigma_{nn'}$(tot)	3	4	0.575 to 15 MeV	0.575 to 20.0 MeV
$\sigma_{n,2n}$	3	16	12.24-15.0 MeV	8.094 to 20.0 MeV
$\sigma_{n,n'He^4}$	3	22	--	8.081 to 20.0 MeV
$\sigma_{n,n'p}$	3	28	10.6-15.0 MeV	9.774 to 20.0 MeV
$\sigma_{nn'}$(discrete)	3	51-90	11 Levels (Threshold to 3.31 MeV)	40 levels (Threshold to 20.0 MeV)
$\sigma_{nn'}$(continuum)	3	91	2.0 to 15.0 MeV	1.86 to 20.0 MeV
$\sigma_{n\gamma}$	3	102	Same as MT=1	Same as MT=1
σ_{np}	3	103	3.5 to 15.0 MeV	0.262 to 20.0 MeV
σ_{nd}	3	104	--	7.507 to 20.0 MeV

Table 1 (contd.)

Neutron Reactions	MF	MT	ENDF/III	ENDF/IV
σ_{nt}	3	105	--	10.15 to 20.0 MeV
σ_{n,He^3}	3	106	--	8.795 to 20.0 MeV
σ_{n,He^4}	3	107	--	10^{-5} to 20.0 MeV (Exothermic)
$\frac{d.\sigma}{d\Omega}_{el}$	4	2	Transformation matrix & $\frac{d\sigma}{d\Omega}$ (tabulated angular distribution) for 67 energies Energy Range 10^{-5} to 15.0 MeV (No data between 2.35 & 14.0 MeV)	Transformation Matrix given Legendre Coeffs (P_ℓ) for 272 Energies 10^{-5} to 20.0 MeV
$\frac{d\sigma_{nn'}}{d\Omega}$	4	4	Isotropic distribution (11 levels & continuum)	Isotropic distribution (40 levels & continuum
n-2n	5	16	Maxwelliam Spectrum	Maxwelliam Spectrum
$n,n'4e^4$	5	22	--	Maxwelliam Spectrum
n,n'p	5	28	Maxwelliam Spectrum	Maxwelliam Spectrum
n,n' (continuum)	5	91	Maxwelliam Spectrum	Tabulated energy distribution
Photon Production and Interaction Data	12	102	--	Multiplication for Photon Production Cross Sections
	13	3	--	Photon Production Cross Sections
	14	3	--	Photon Angular Distribution(Isotropic)
	14	102	--	Photon Angular Distribution(Isotropic)
	15	3	--	Continuous Photon Energy Spectra
	15	102	--	Continuous Photon Energy Spectra

Table 2

Cr^{50} Q-Values

Reaction	-Q(MeV)	ENDF MT
(n,p)	0.257	103
(n,He^3)	8.628	106
(n,n'd)	18.92	
(n,n'He^4)	8.555	22
(n,He^4n')	8.555	22
(n,p,He^4)	10.139	
(n,2n)	12.939	16
(n,d)	7.364	104
(n,He^4)	-0.322	107
(n,n't)	23.20	
(n,p,n')	9.588	28
(n,He^4,p)	10.14	
(n,3n)	23.581	17
(n,t)	12.662	105
(n,n'p)	9.59	28
(n,n'He^3)	20.255	
(n,2p)	8.204	
(n,d,n)	18.919	

% Abundance = 4.35
Mass = 49.9460488 amu
Binding energy of last neutron in compound nucleus = 9.262 MeV

Table 3

Cr^{52} Q-Values

Reaction	-Q(MeV)	ENDF MT
(n,p)	3.196	103
(n,He^3)	10.844	106
(n,n'd)	19.335	
(n,n'He^4	9.353	22
(n,He^4n')	9.353	22
(n,p,He^4)	12.562	
(n,2n)	12.041	16
(n,d)	8.282	104
(n,He^4)	1.2108	107
(n,n't)	22.409	
(n,p,n')	10.507	28
(n,He^4,p)	12.562	
(n,3n)	21.302	17
(n,t)	13.077	105
(n,n'p)	10.507	28
(n,n'He^3)	21.788	
(n,2p)	12.190	
(n,d,n)	19.335	

% Abundance = 83.79
Mass = 51.9405102 amu
Binding Energy of last neutron in compound nucleus = 7.940 MeV

Table 4

Cr^{53} Q-Values

Reaction	-Q(MeV)	ENDF MT
(n,p)	2.640	103
(n,He^3)	12.412	106
(n,n'd)	16.222	
(n,n'He^4)	9.15	22
(n,He^4n')	9.151	22
(n,p,He^4)	10.374	
(n,2n)	7.940	16
(n,d)	8.911	104
(n,He^4)	-1.794	107
(n,n't)	21.017	
(n,p,n')	11.136	28
(n,He^4,p)	10.374	
(n,3n)	19.981	17
(n,t)	9.965	105
(n,n'p)	11.136	28
(n,n'He^3)	18.784	
(n,2p)	12.323	
(n,d,n)	16.222	

% Abundance = 9.50
Mass = 52.940651 amu
Binding energy of last neutron in compound nucleus = 9.720 MeV

Table 5

Cr^{54} Q-Values

Reaction	-Q(MeV)	ENDF MT
(n,p)	6.220	103
(n,He^3)	14.325	106
(n,n'd)	18.631	
(n,n'He^4)	7.927	22
(n,He^4n')	7.927	2
(n,p,He^4)	14.031	
(n,2n)	9.720	16
(n,d)	10.135	104
(n,He^4)	1.554	107
(n,n't)	19.685	
(n,p,n')	12.360	28
(n,He^4,p)	14.031	
(n,3n)	17.660	17
(n,t)	12.374	105
(n,n'p)	12.360	28
(n,n'He^3)	22.132	
(n,2p)	16.8633*	
(n,d,n)	18.631	

% Abundance = 2.36
Mass = 53.9388813 amu
Binding energy of last neutron in compound nucleus = 6.246 MeV

*Based on mass of $_{22}Ti^{53}$ from G. T. Garvey et al. (Rev. Mod. Phys. 41 (2) 1969.

Table 6

Average Capture Cross Section (mb)

Energy Range (keV)	Stieglitz et al	Le Rigoleur
90-100	18.8 ± 3.5	20.8 ± 1.0
100-150	8.8 ± 2.0	9.96 ± 0.45

Table 7

Energy Level Scheme for ^{50}Cr

Level	I^{π}	Excitation (MeV)
0	0^+	0.000
1	2^+	0.783
2	4^+	1.879
3	2^+	2.922
4	2^+	3.160
5	4^+	3.320
6	2^+	3.693
7	5^+	3.787
8	0^+	3.895
9	3^-	4.524
10	2^+	4.653

Table 8

Energy Level Scheme for ^{52}Cr

Level	I^{π}	Excitation (MeV)
0	0^+	0.000
1	2^+	1.434
2	4^+	2.370
3	0^+	2.647
4	4^+	2.768
5	2^+	2.965
6	6^+	3.114
7	2^+	3.162
8	4^+	3.414
9	5^+	3.617
10	2^+	3.771
11	4^+	4.039
12	3^-	4.563
13	4^+	4.630
14	4^+	4.837
15	4^+	5.097
16	2^+	5.292
17	0^+	5.585
18	0^+	5.737
19	2^+	6.070
20	2^+	6.154

Table 8 (contd.)

Level	I^{π}	Excitation (MeV)
21	3^-	6.490
22	2^+	6.820
23	3^-	7.070
24	3^-	7.900

Table 9

Energy Level Scheme for ^{53}Cr

Level	I^{π}	Excitation (MeV)
0	$3/2^-$	0.000
1	$1/2^-$	0.564
2	$5/2^-$	1.006
3	$7/2^-$	1.287
4	$7/2^-$	1.539
5	$7/2^-$	1.973
6	$11/2^-$	2.173
7	$9/2^-$	2.233
8	$3/2^-$	2.321
9	$5/2^-$	2.661
10	$11/2^-$	2.827
11	$15/2^-$	3.084
12	$7/2^-$	3.352
13	$13/2^-$	3.593
14	$9/2^+$	3.713
15	$3/2^+$	3.982

Table 10

Energy Level Scheme for ^{54}Cr

Level	I^{π}	Excitation (MeV)
0	0^+	0.000
1	2^+	0.835
2	4^+	1.827
3	2^+	2.619
4	0^+	2.829
5	2^+	3.074
6	2^+	3.437
7	4^+	3.487
8	4^+	3.800
9	0^+	4.015
10	3^-	4.129
11	0^+	4.573

Table 11

Comparison of Total and Elastic Cross Sections

	Cr(Nat) Ref (16)		Cr(Nat) Ref (17)		Cr(Nat) ENDF/IV		^{52}Cr (O.M. Calc.)	
E(MeV)	σ_t(b)	σ_{el}(b)	σ_t(b)	σ_{el}(b)	σ_t(b)	σ_{el}(b)	σ_t(b)	σ_{el}(b)
4.00	3.75 ± 0.06	2.21 ± 0.11	-	-	3.85	2.63	3.77	2.35
4.34	-	-	3.74 ± 0.037	2.44 ± 0.18	3.64	2.35	3.77	2.35
4.56	3.75 ± 0.06	2.44 ± 0.12	-	-	3.87	2.51	3.80	2.35
4.92	-	-	3.92 ± 0.39	2.44 ± 0.18	3.79	2.32	3.74	2.33
5.50	3.66 ± 0.07	1.99 ± 0.16	-	-	3.65	2.17	3.70	2.27
6.09	3.66 ± 0.08	2.00 ± 0.10	-	-	3.58	2.11	3.65	2.19
				2.23 ± 0.16[a]				
6.44	-	-	3.56 ± 0.036	2.18 ± 0.16	3.54	2.08	3.59	2.13
7.05	3.38 ± 0.08	1.83 ± 0.09	-	-	3.46	2.02	3.50	2.03
				1.89 ± 0.14[a]				
7.54	-	-	3.34 ± 0.033	1.915 ± 0.14	3.38	1.96	3.41	1.93
8.05	3.19 ± 0.08	1.78 ± 0.09	-	-	3.28	1.89	3.32	1.83
				1.69 ± 0.12				
8.56	-	-	3.16 ± 0.031	1.79 ± 0.134	3.16	1.79	3.14	1.69
10.0	-	-			2.88	1.52	2.89	1.44
14.0	-	-			2.42	1.11	2.43	1.01
20.0	-	-			2.00	0.73	2.17	0.90

[a] ^{52}Cr

Table 12

Error Estimates of the Evaluated Cross Sections of Cr

Cross Section	ENDF/B Designation MF	MT	Neutron Energy (MeV) Thermal	Resonance 10^{-11}-0.65	1	2	3	5	10	15	20
Total	3	1	5%	10%	2%	2%	2%	2%	2%	2%	2%
Elastic	3	2	5%	15-30%	15%	10%	10%	5%	8%	10%	10%
Non-Elastic	3	3	5%	15-30%	15%	10%	10%	5%	8%	10%	10%
Total (n,n')	3	51	-	-	15%	10%	10%	15%	40%	40%	40%
Discrete (n,n')*	3	52	-	-	20%	20%	20%	20%	30%	30%	30%
"	3	53	-	-	20%	15%	15%	15%	30%	30%	30%
"	3	54	-	-	30%	15%	15%	20%	30%	30%	30%
"	3	55	-	-	-	15%	15%	20%	30%	30%	30%
"	3	56	-	-	-	15%	10%	10%	20%	20%	20%
"	3	57	-	-	-	20%	15%	15%	20%	30%	30%
"	3	58	-	-	-	40%	20%	15%	15%	20%	20%
"	3	62	-	-	-	-	25%	15%	15%	20%	20%
"	3	63	-	-	-	-	30%	20%	20%	30%	30%
Other Discrete (n,n')	3	59-90	-	-	-	50%	50%	40%	40%	40%	40%

*Experimental data exists for these levels.

Table 12 (Contd.)

Cross Section	ENDF/B Designation MF	MT	Neutron Energy (MeV) Thermal	Resonance 10^{-11}-0.65	1	2	3	5	10	15	20
Continuum (n,n')	3	91	-	-	-	50%	50%	40%	40%	40%	40%
(n,2n)	3	16	-	-	-	-	-	-	20%	15%	20%
(n,n'α)	3	22	-	-	-	-	-	-	100%	100%	100%
(n,n'p)	3	28	-	-	-	-	-	-	150%	100%	100%
(n,γ)	3	102	5%	15-30%	20%	20%	20%	15%	15%	10%	20%
(n,p)	3	103	-	-	100%	100%	100%	75%	50%	50%	50%
(n,d)	3	104	-	-	-	-	-	-	200%	200%	200%
(n,t)	3	105	-	-	-	-	-	-	400%	400%	400%
(n,He^3)	3	106	-	-	-	-	-	-	400%	400%	400%
(n,α)	3	107	-	-	-	-	200%	100%	75%	30%	50%
Gamma Prod. (n,γ)	12	102	30%	30%	-	-	-	-	-	-	-
(n,xγ)	13	3	-	-	20%	20%	20%	20%	20%	20%	20%

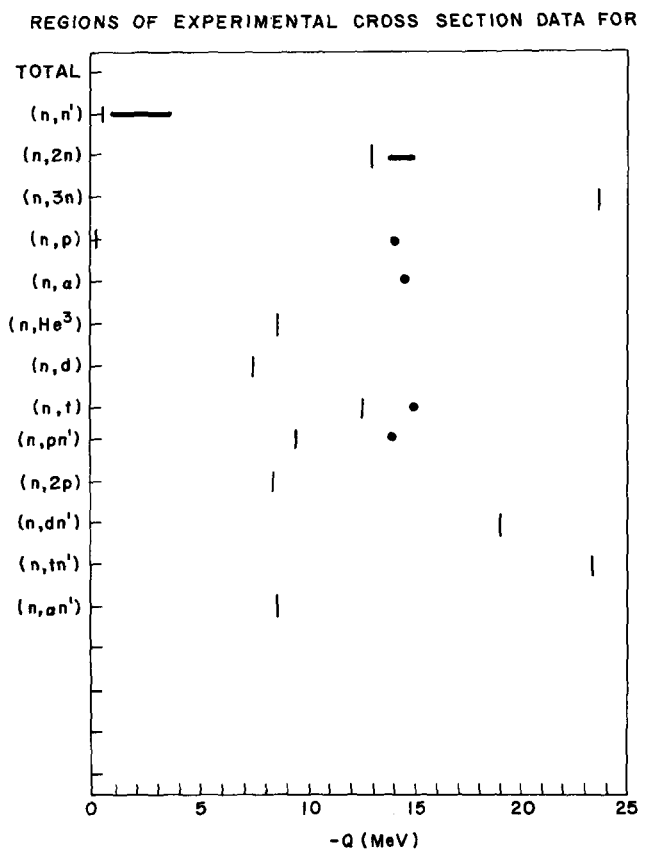

Figure 1.

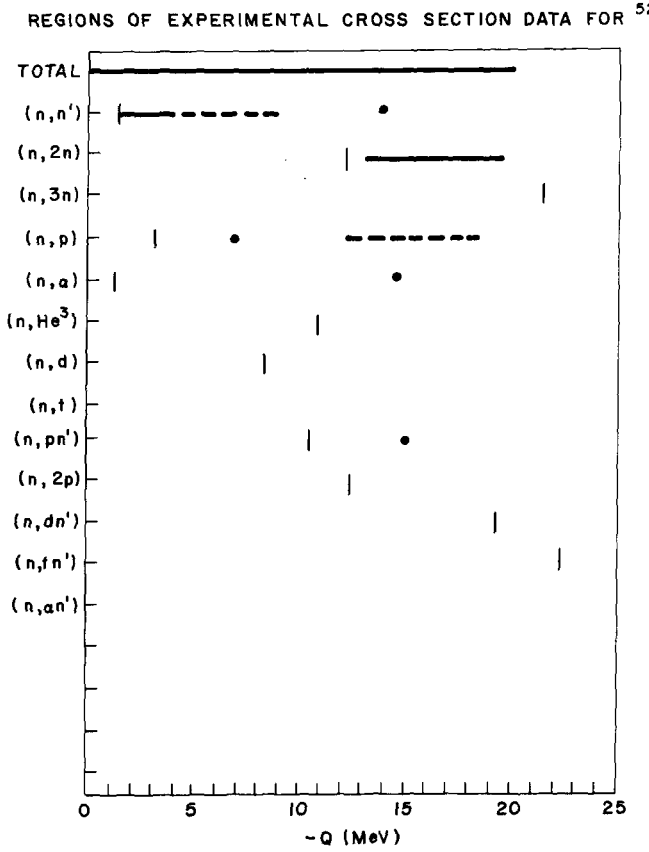

Figure 2.

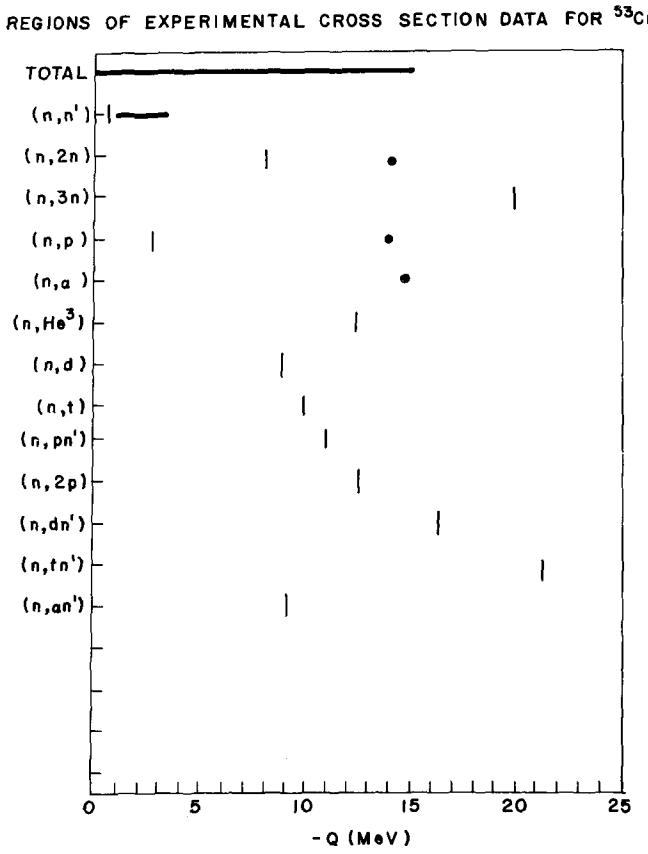

Figure 3.

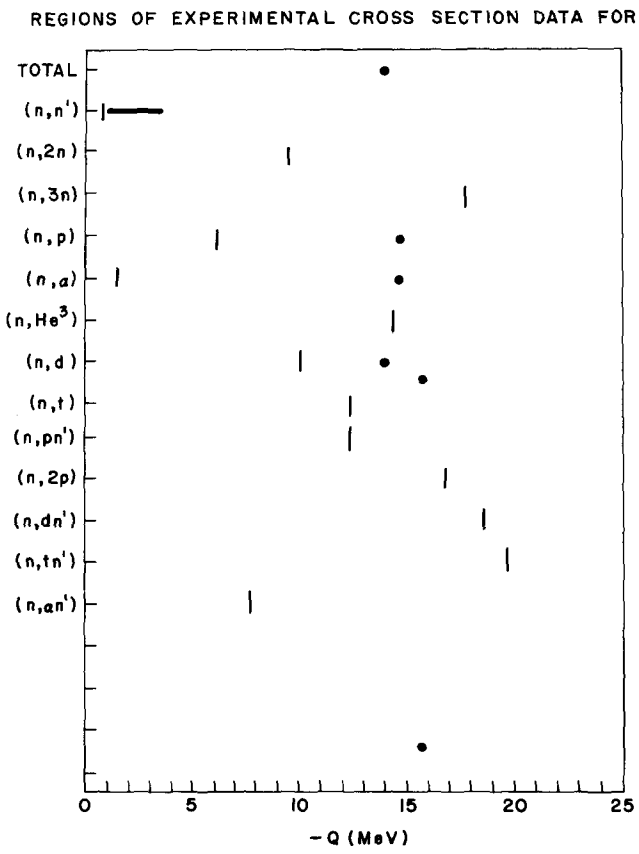

Figure 4.

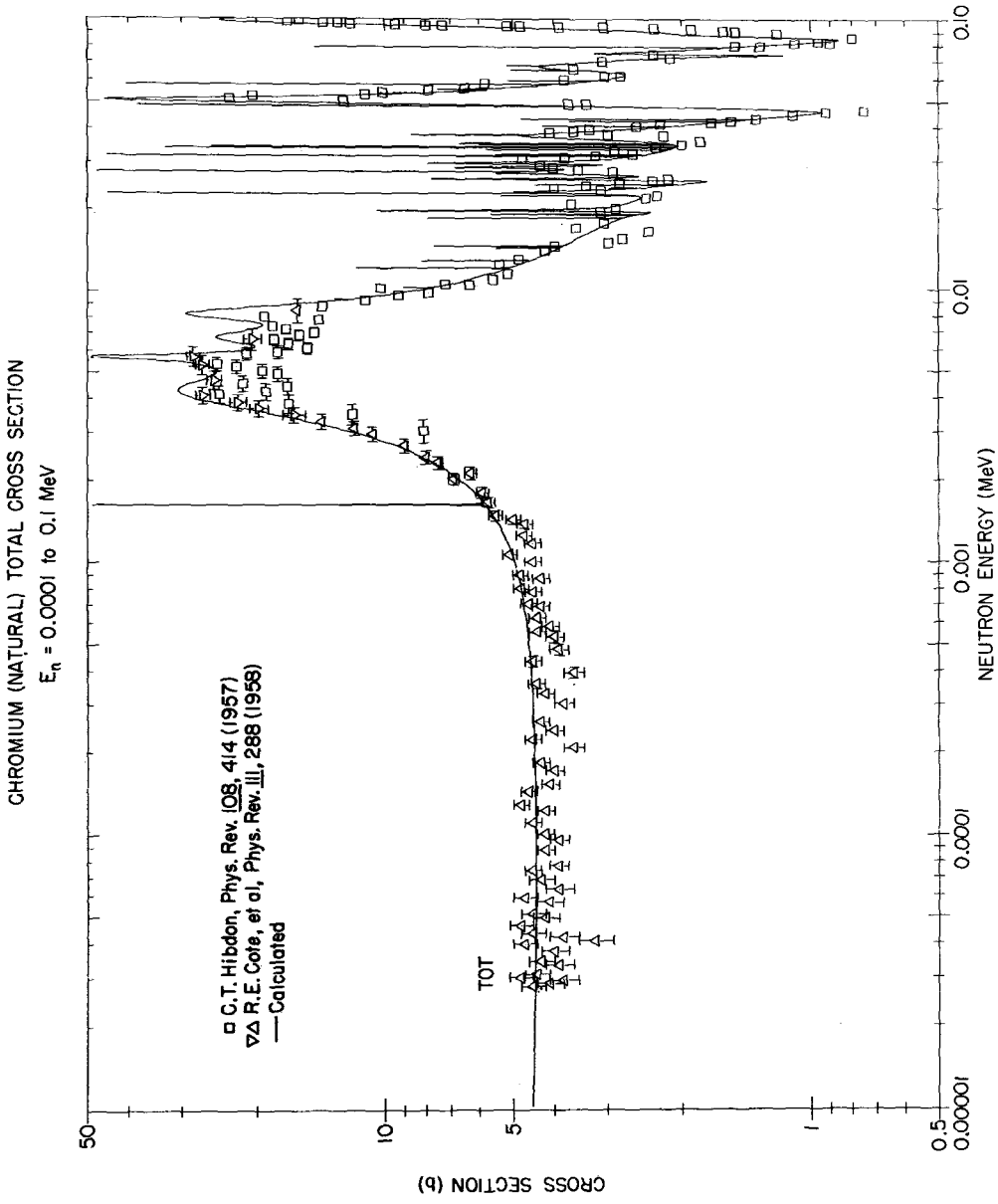
CHROMIUM (NATURAL) TOTAL CROSS SECTION
E_n = 0.0001 to 0.1 MeV
□ C.T. Hibdon, Phys. Rev. 108, 414 (1957)
▽△ R.E. Cote, et al, Phys. Rev. 111, 288 (1958)
— Calculated
TOT
CROSS SECTION (b)
NEUTRON ENERGY (MeV)
50
10
5
1
0.5
0.00001
0.0001
0.001
0.01
0.10

Figure 5.

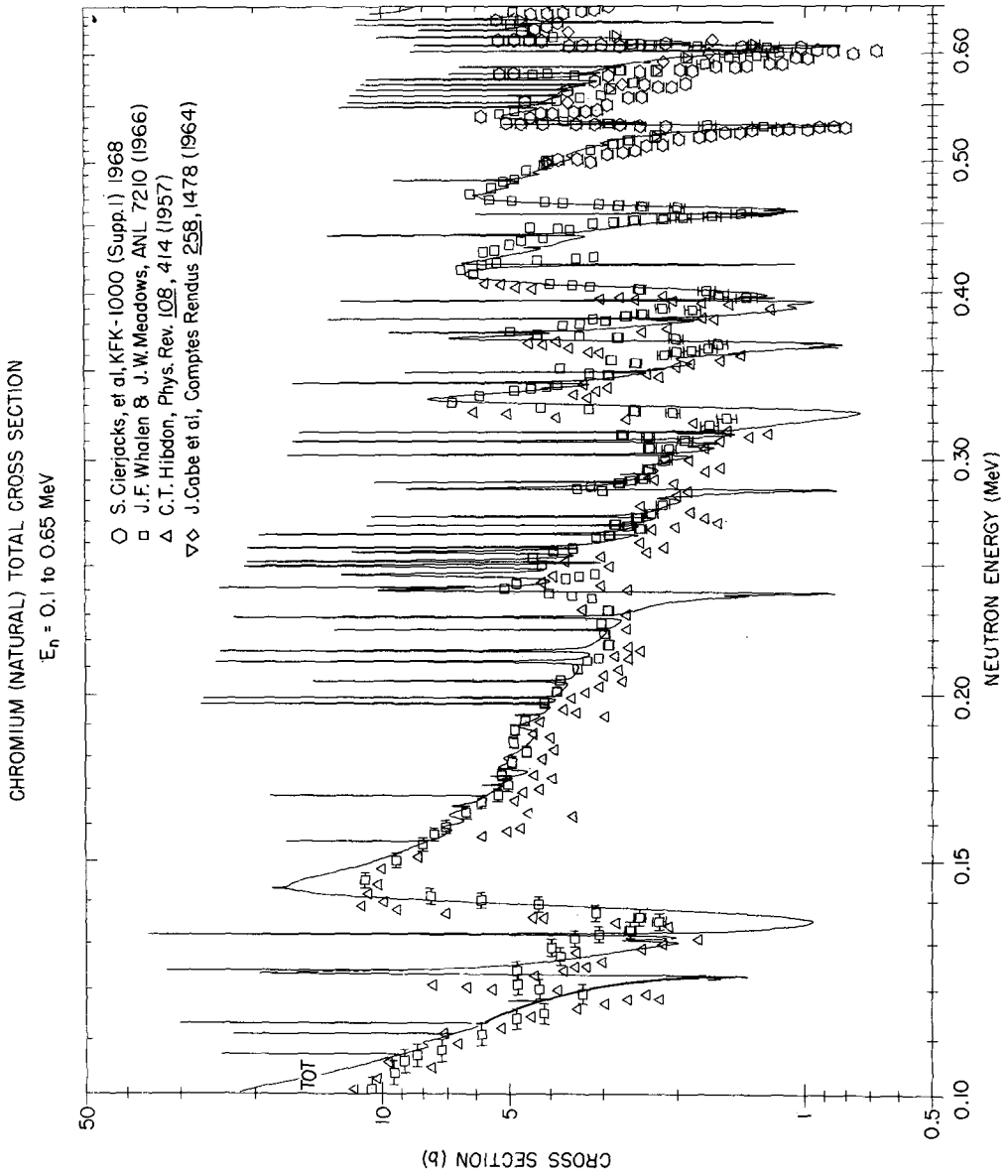
CHROMIUM (NATURAL) TOTAL CROSS SECTION
E_n = 0.1 to 0.65 MeV
○ S.Cierjacks, et al, KFK-1000 (Supp.1) 1968
□ J.F. Whalen & J.W.Meadows, ANL 7210 (1966)
△ C.T. Hibdon, Phys. Rev. 108, 414 (1957)
▽◇ J.Cabe et al, Comptes Rendus 258, 1478 (1964)
TOT
CROSS SECTION (b)
50
10
5
1
0.5
0.10
0.15
0.20
0.30
0.40
0.50
0.60
NEUTRON ENERGY (MeV)

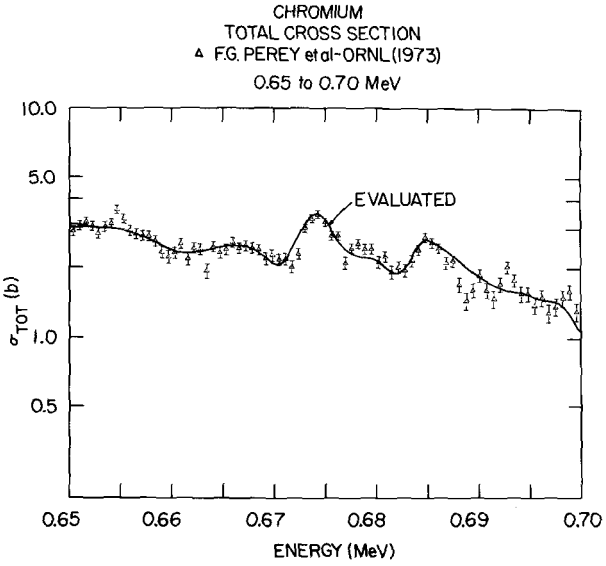

Figure 7.

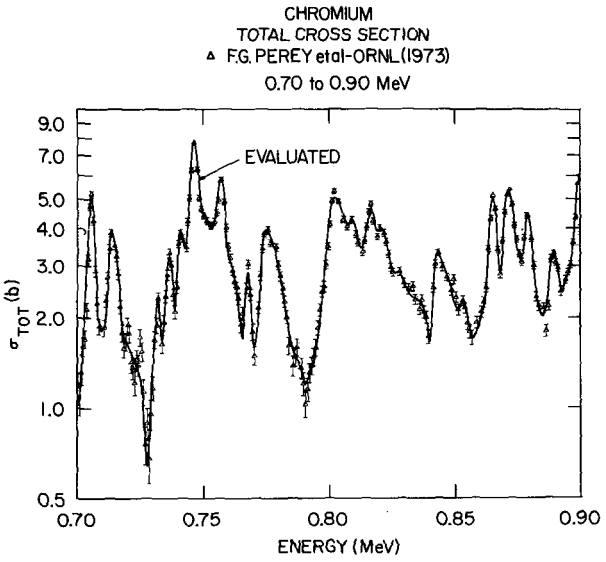

Figure 8.

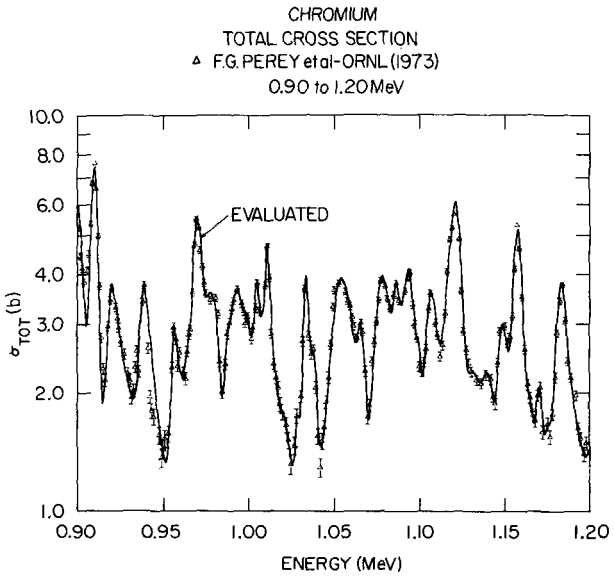

Figure 9.

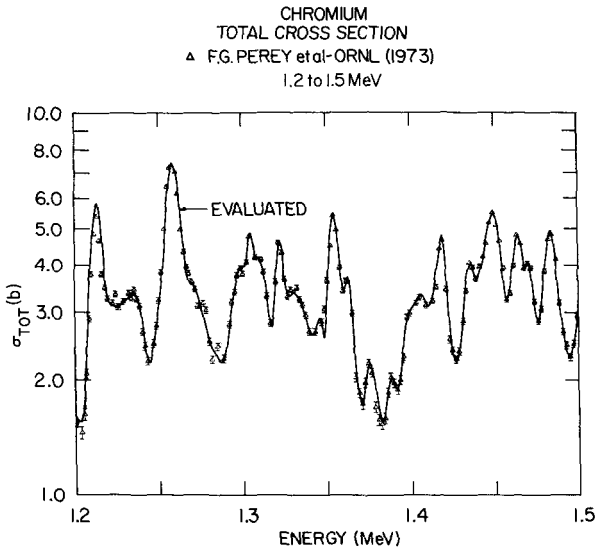

Figure 10.

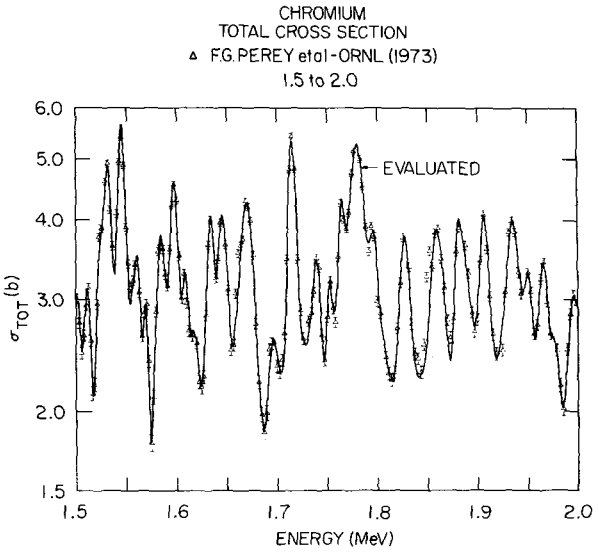

Figure 11.

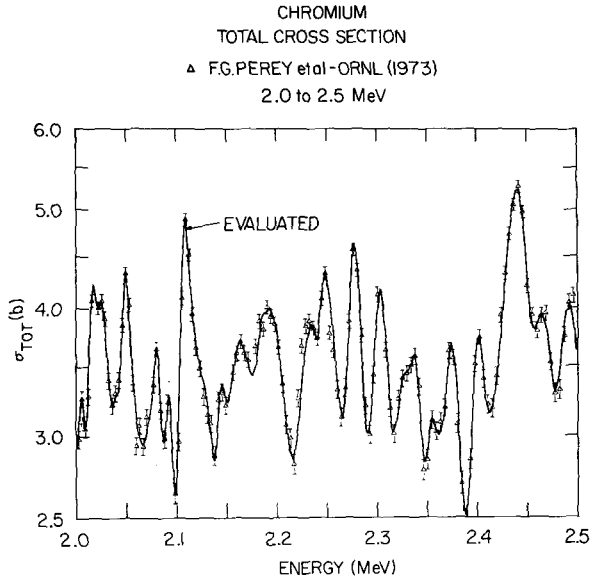

Figure 12.

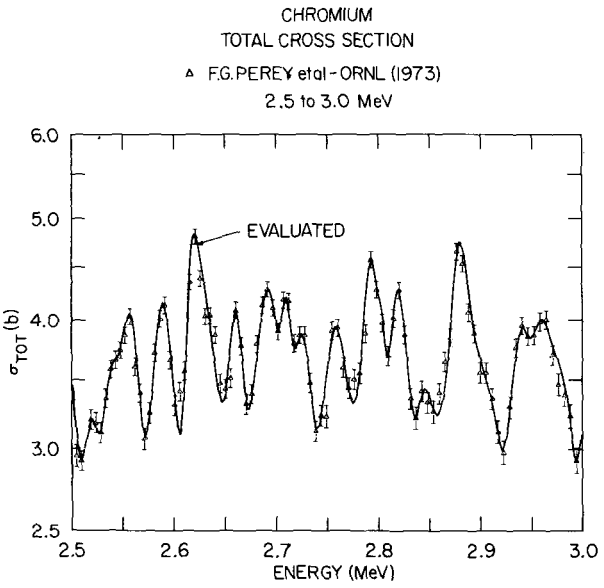

Figure 13.

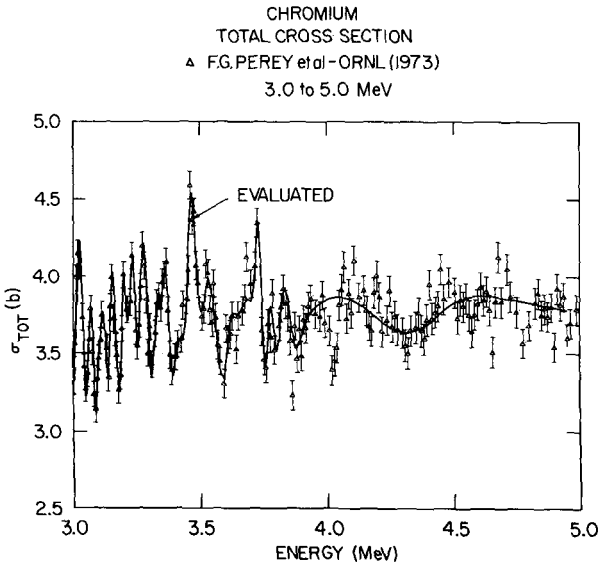

Figure 14.

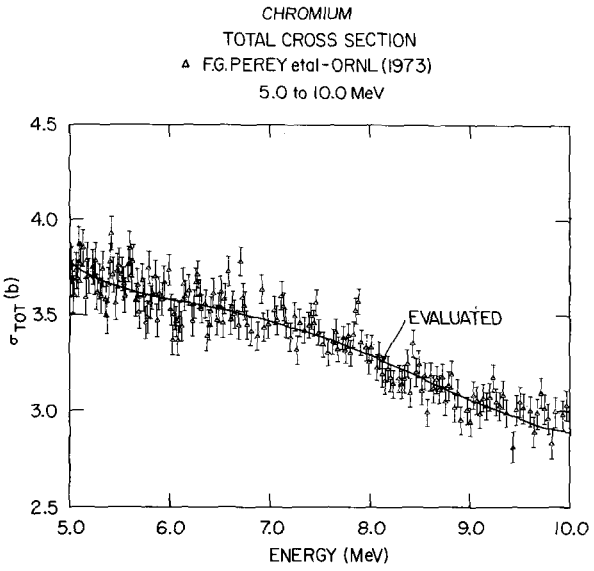

Figure 15.

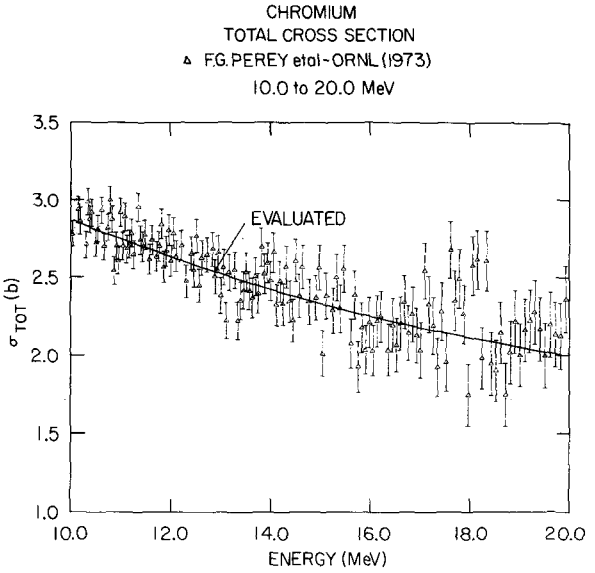

Figure 16.

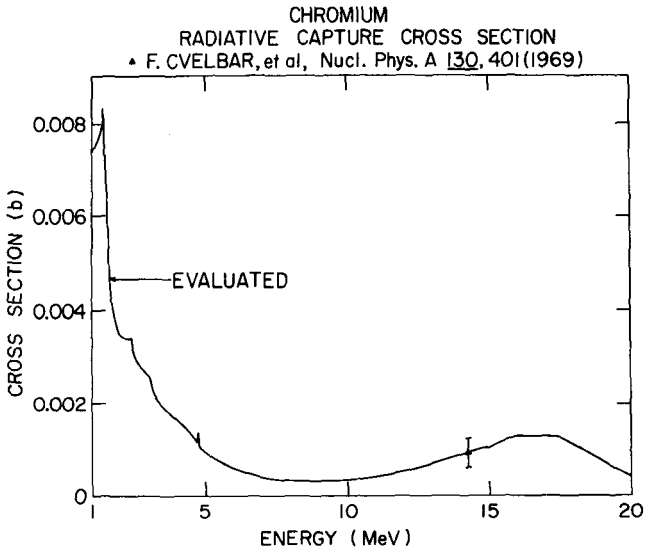

Figure 17.

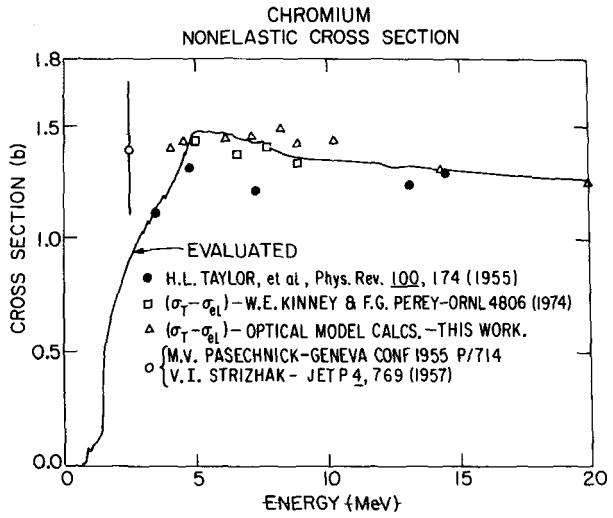

Figure 18.

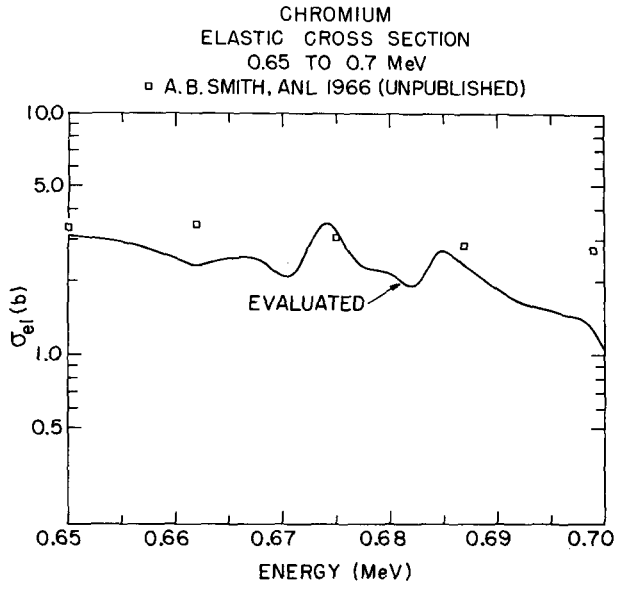

Figure 19.

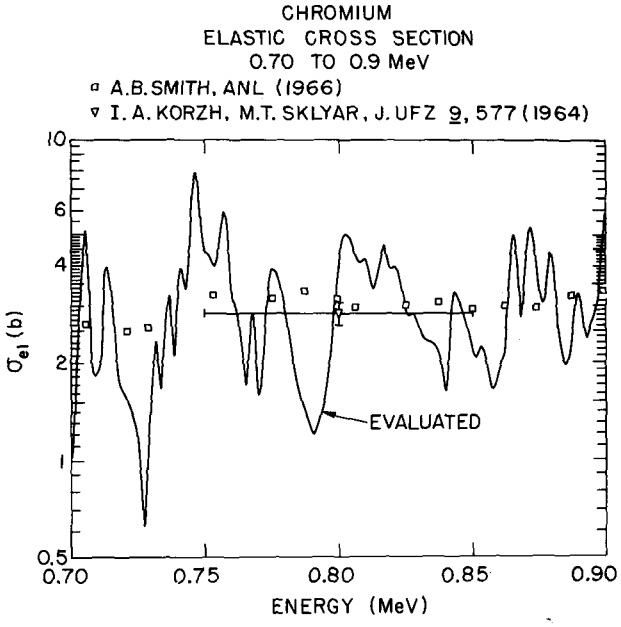

Figure 20.

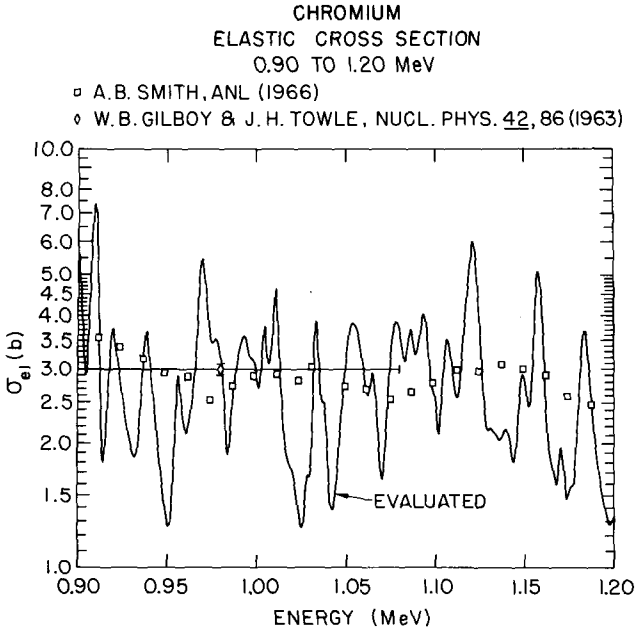

Figure 21.

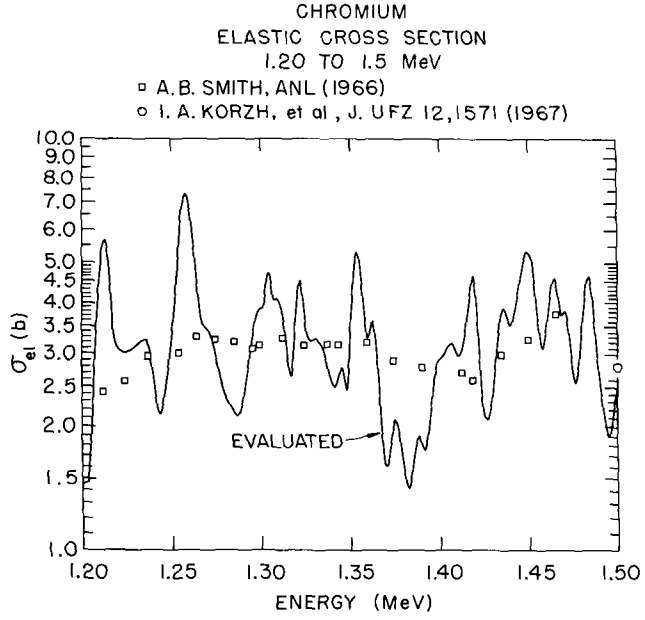

Figure 22.

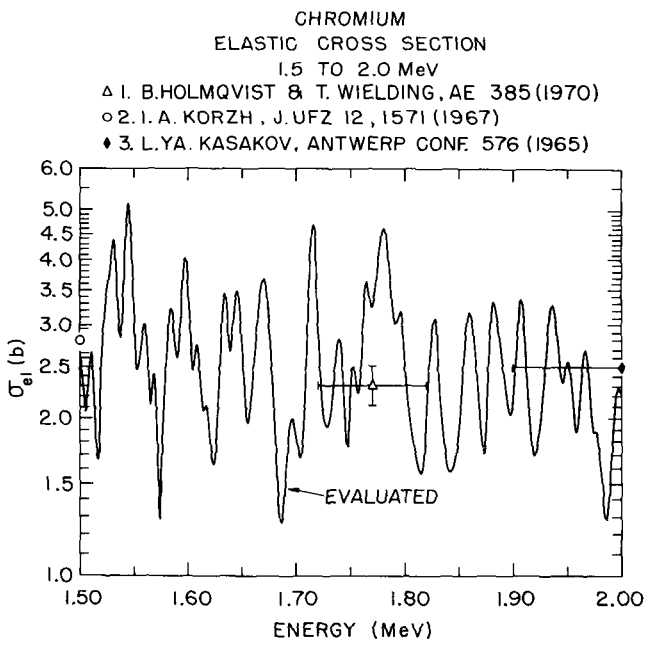

Figure 23.

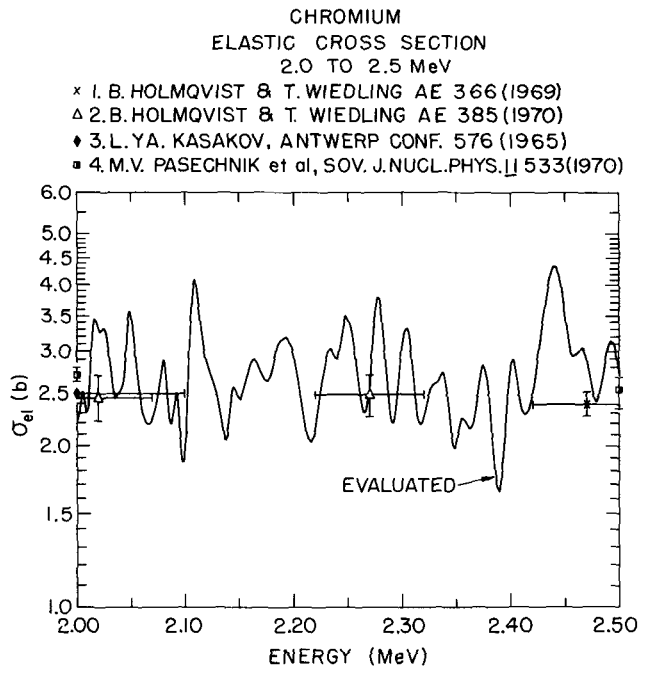

Figure 24.

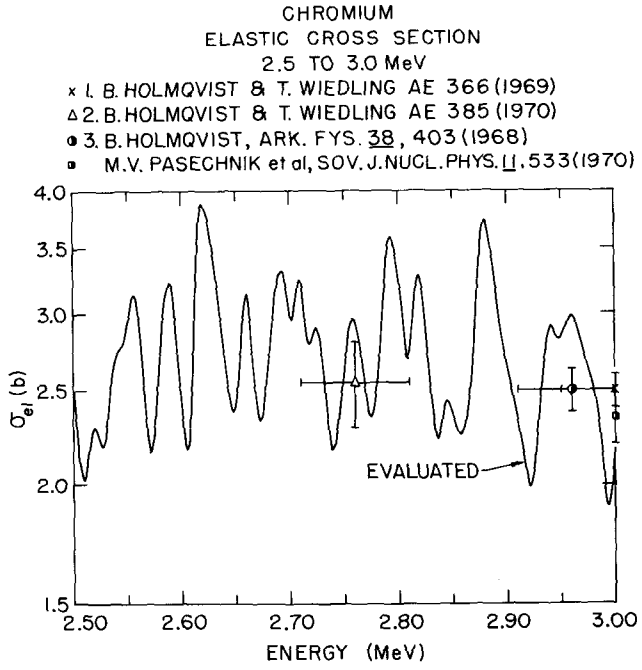

Figure 25.

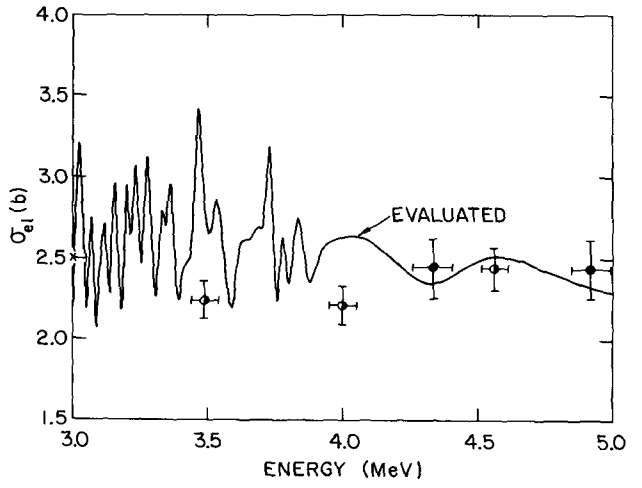

Figure 26.

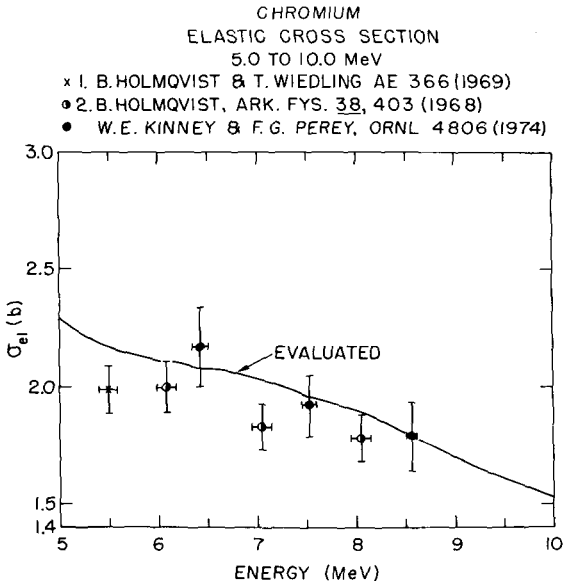

Figure 27.

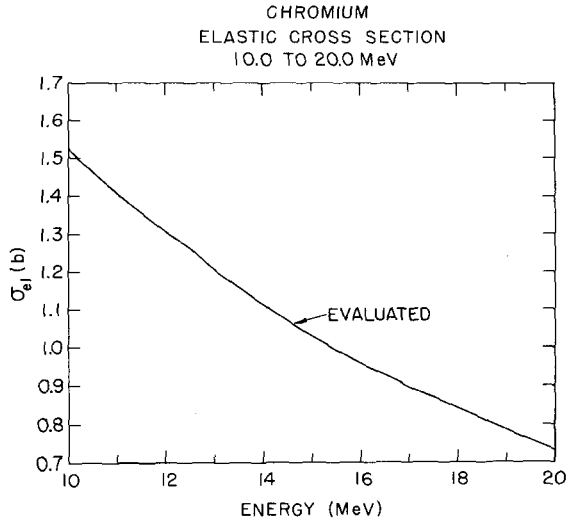

Figure 28.

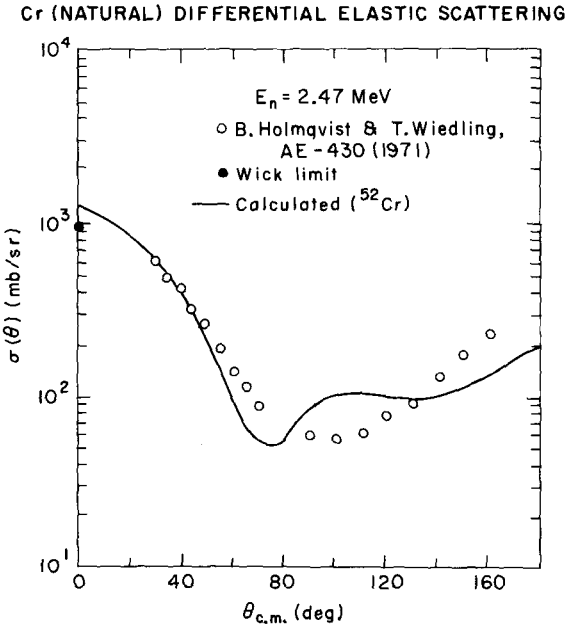

Figure 29.

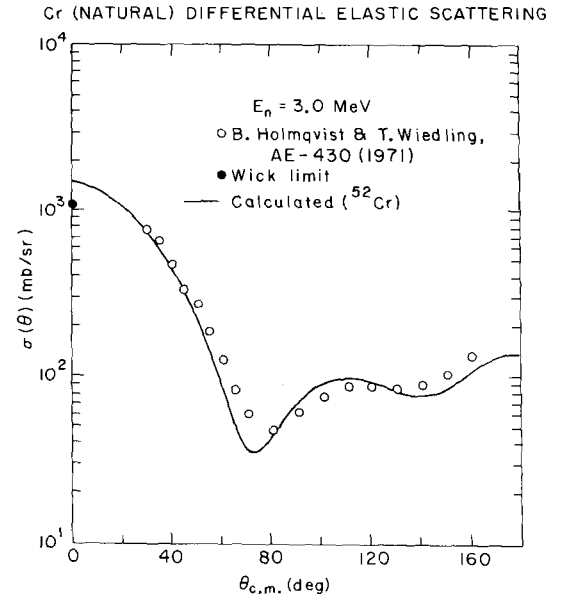

Figure 30.

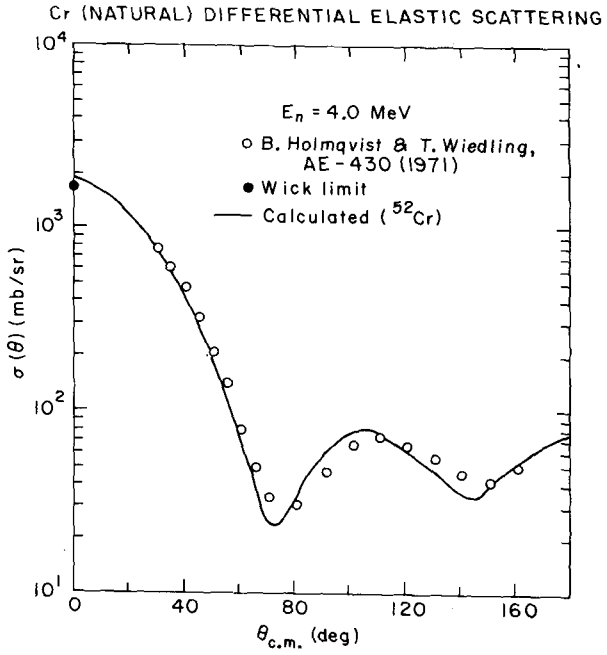

Figure 31.

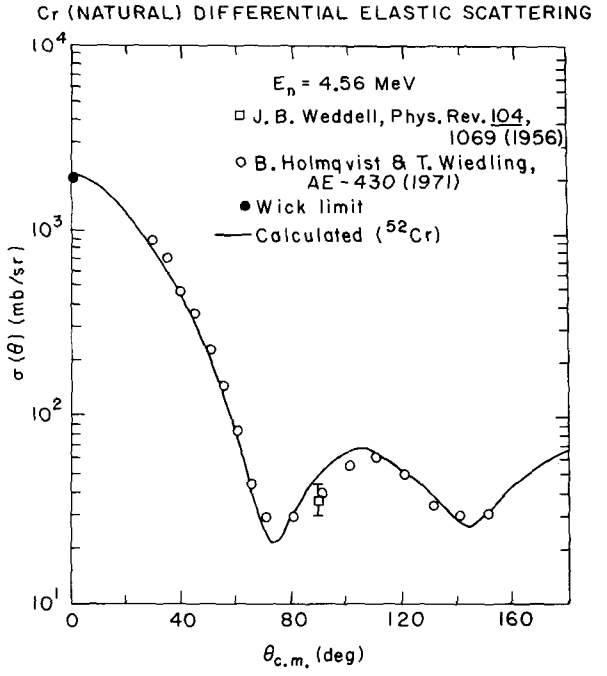

Figure 32.

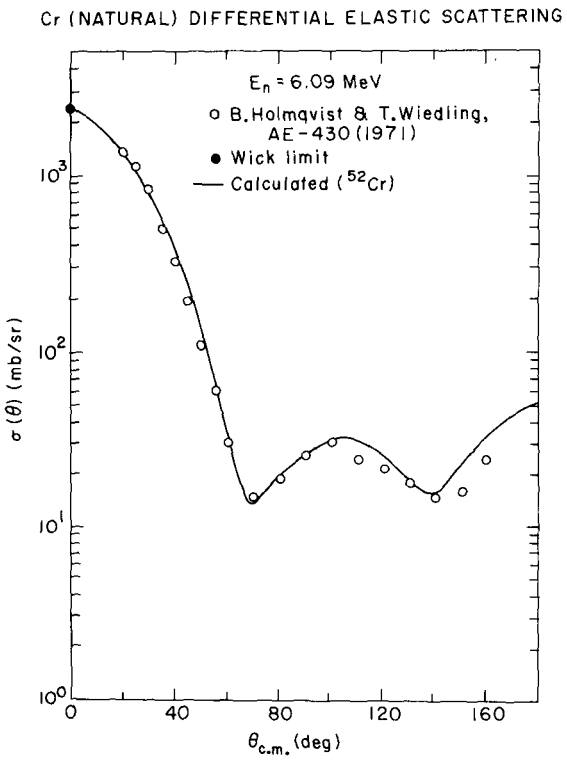

Figure 33.

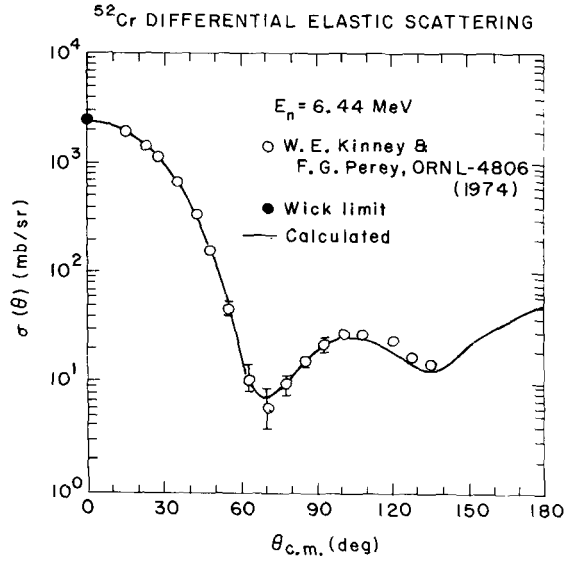

Figure 34.

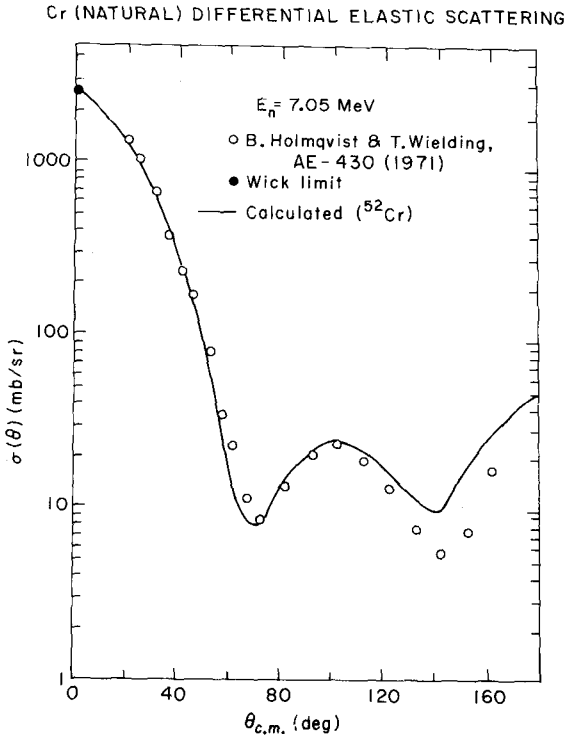

Figure 35.

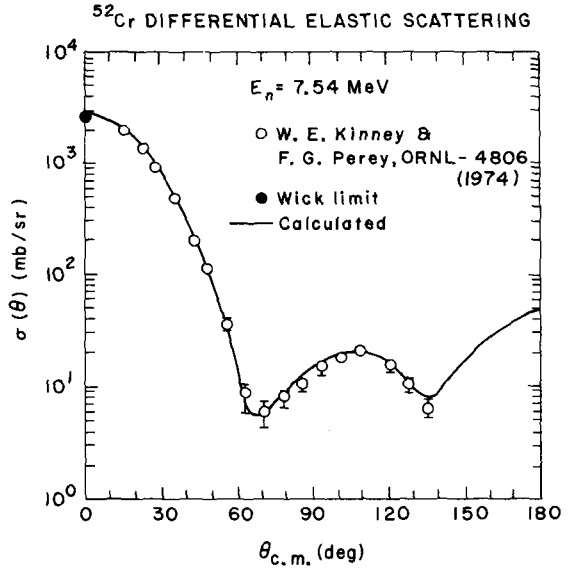

Figure 36.

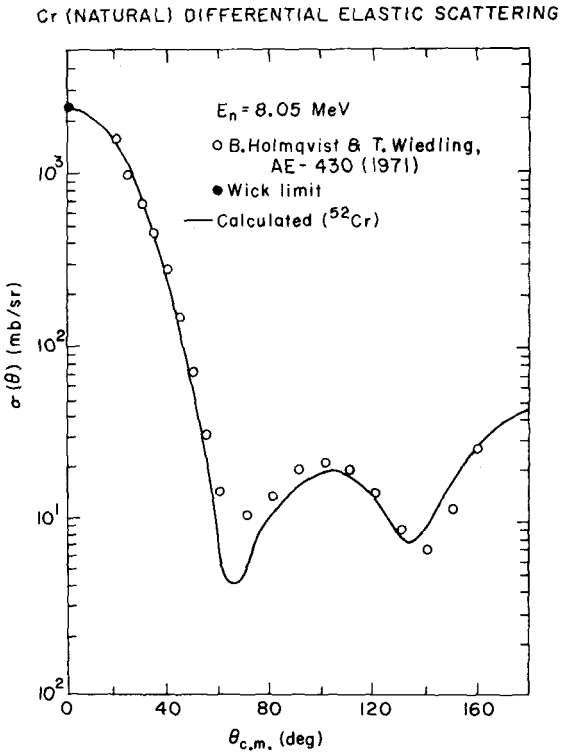

Figure 37.

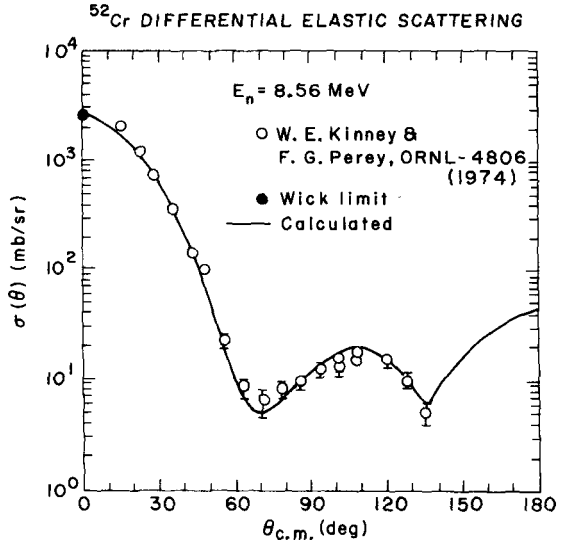

Figure 38.

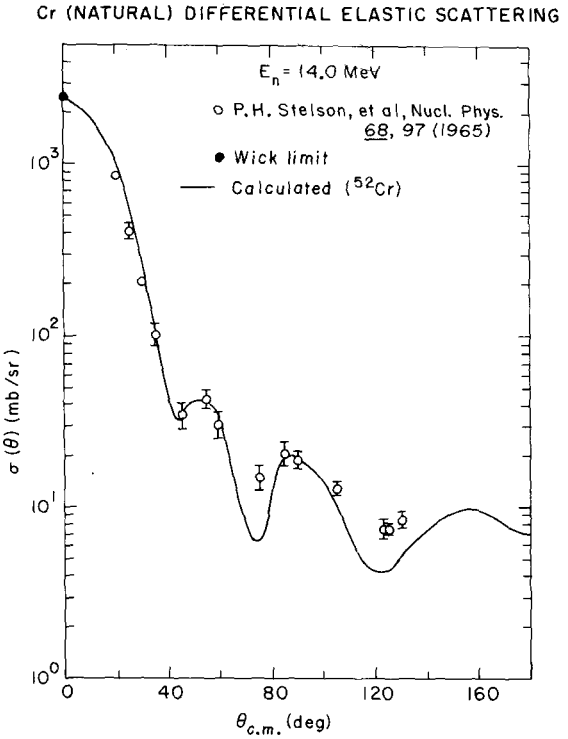

Figure 39.

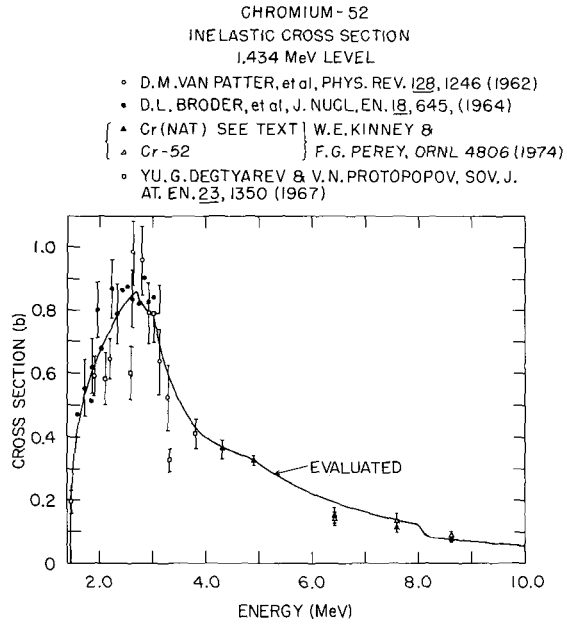

Figure 40.

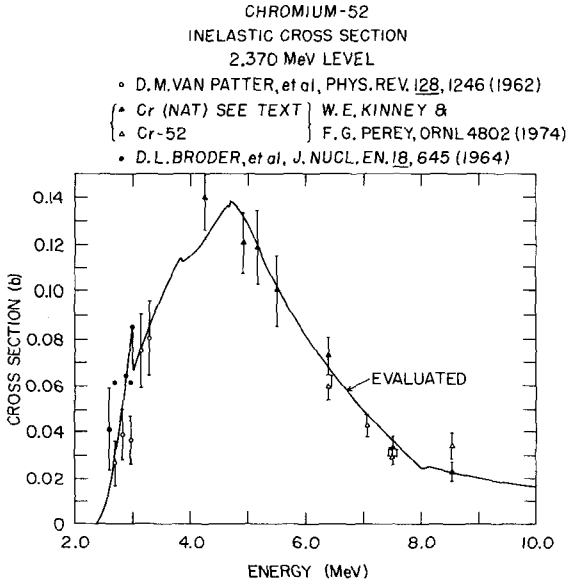

Figure 41.

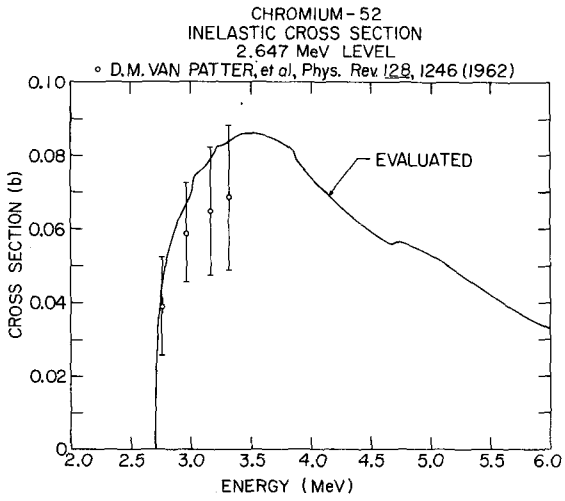

Figure 42.

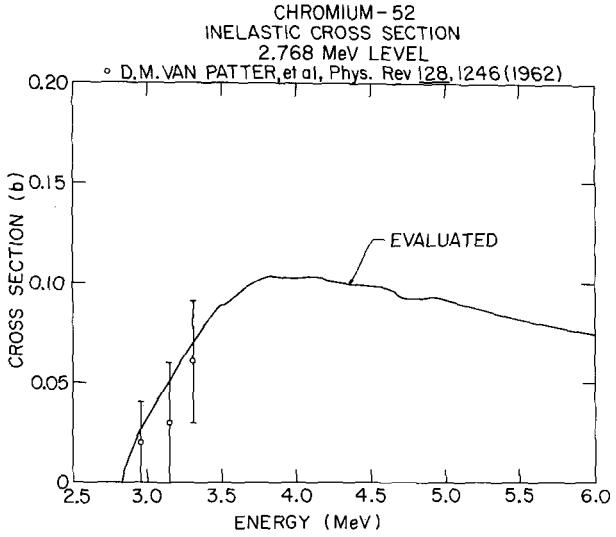

Figure 43.

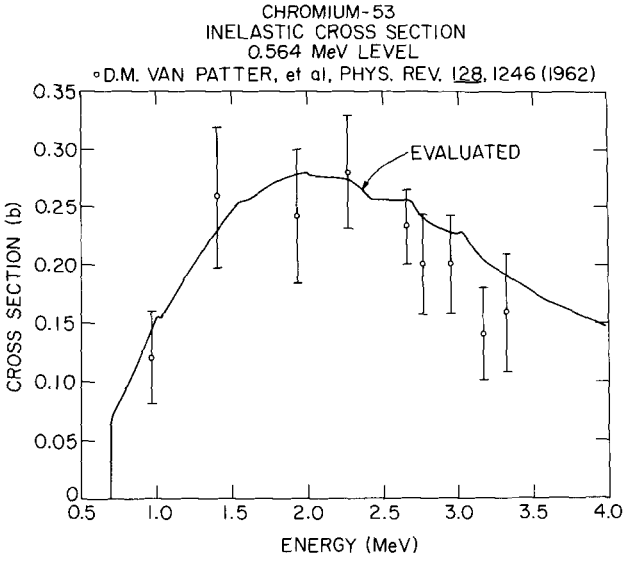

Figure 44.

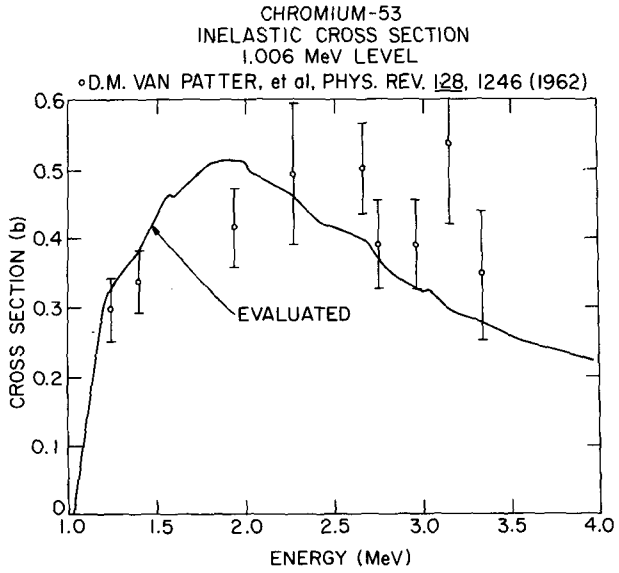

Figure 45.

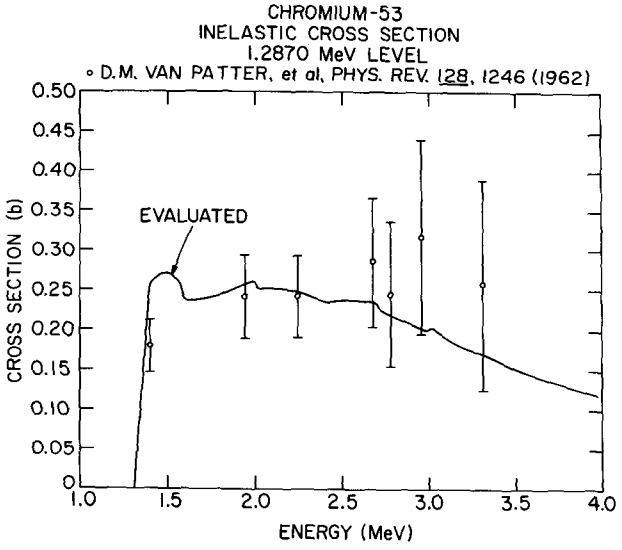

Figure 46.

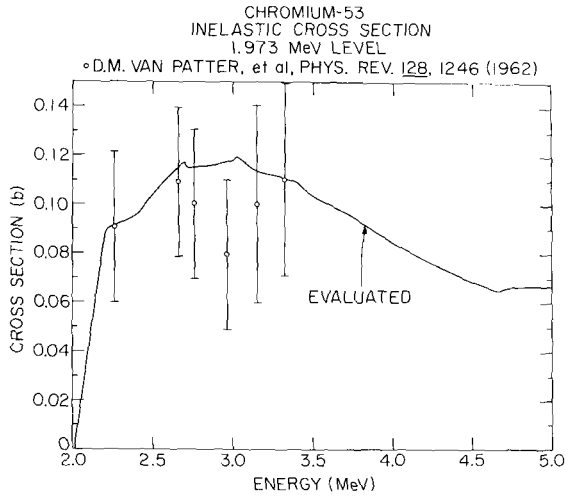

Figure 47.

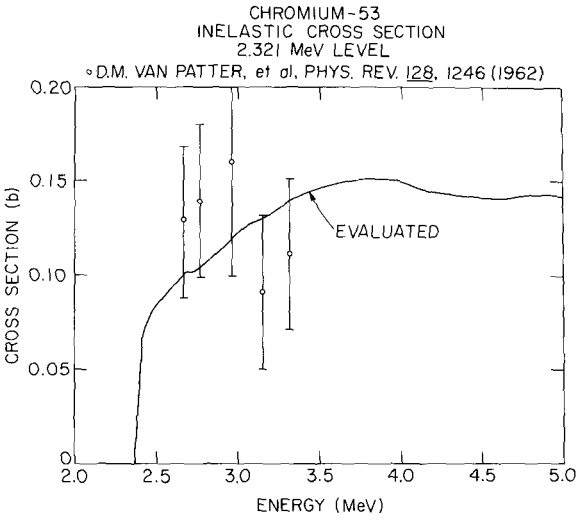

Figure 48.

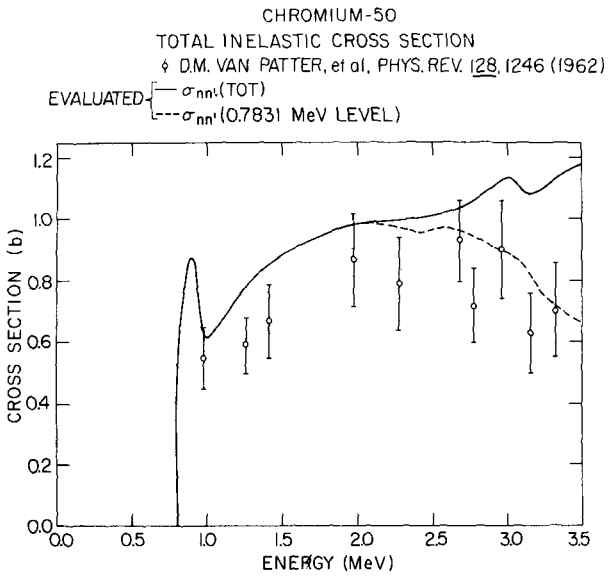

Figure 49.

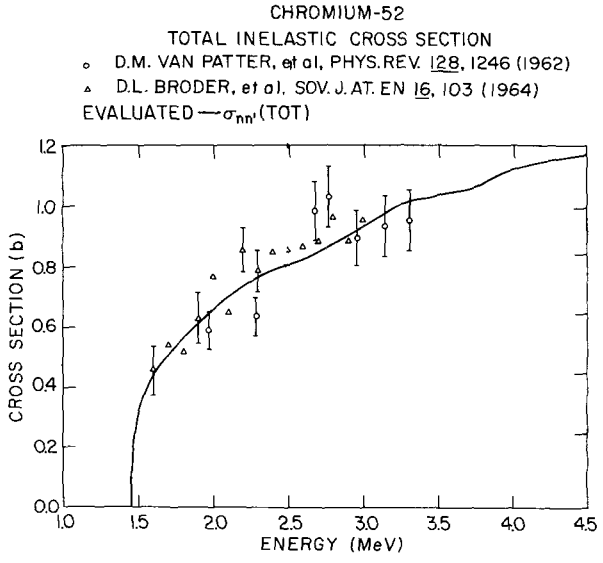

Figure 50.

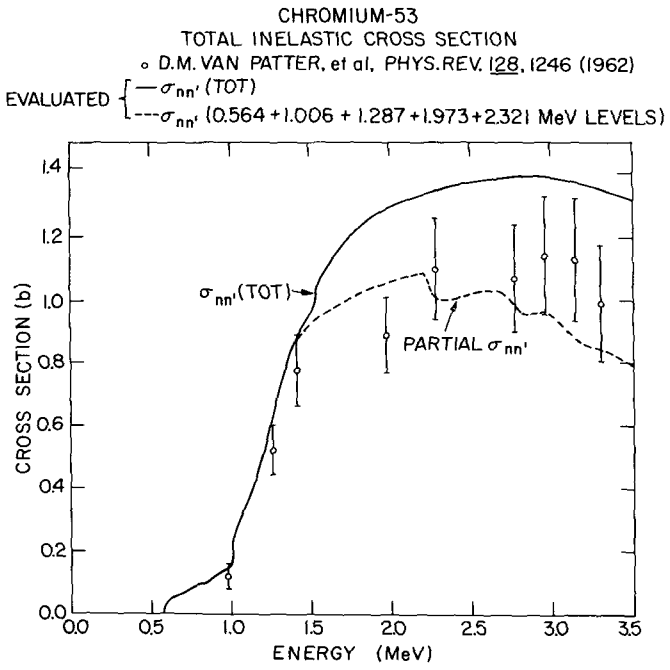

Figure 51.

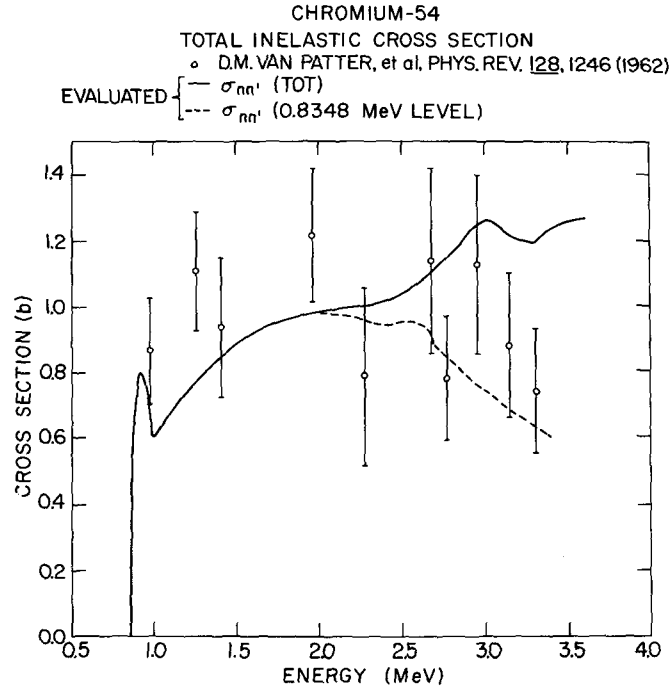

Figure 52.

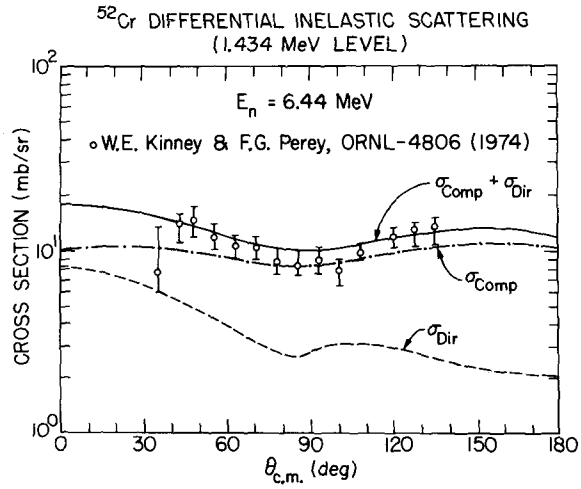

Figure 53.

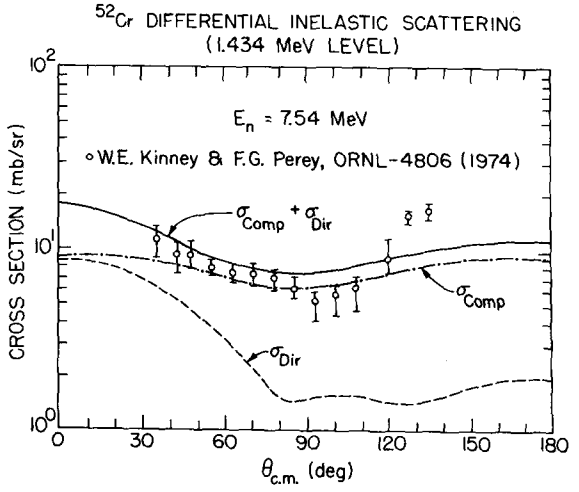

Figure 54.

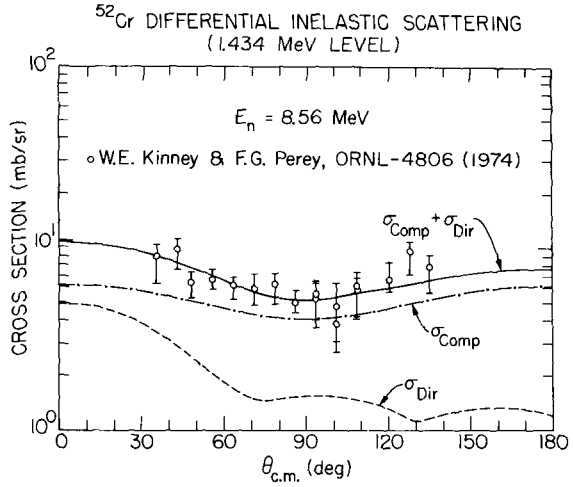

Figure 55.

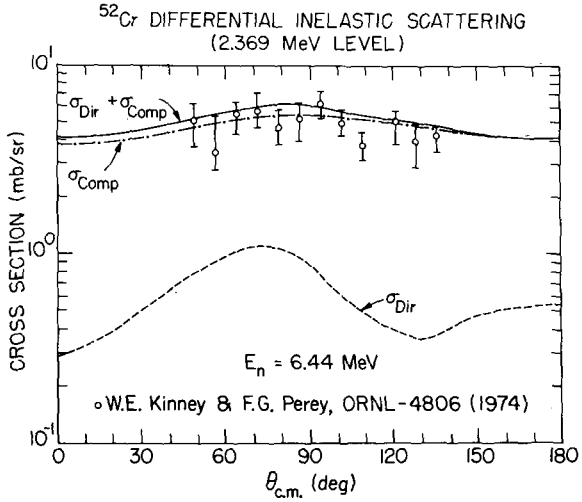

Figure 56.

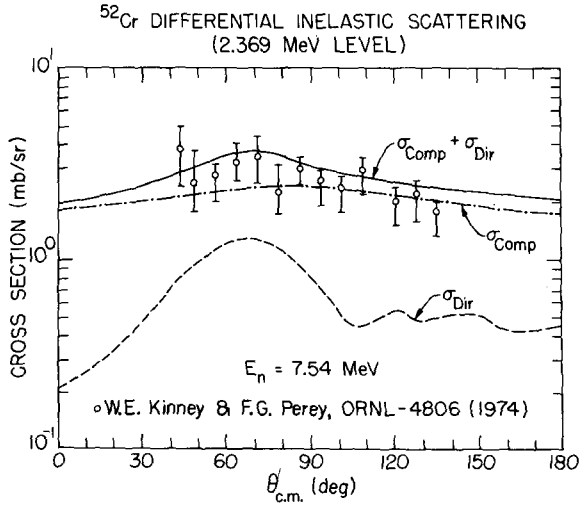

Figure 57.

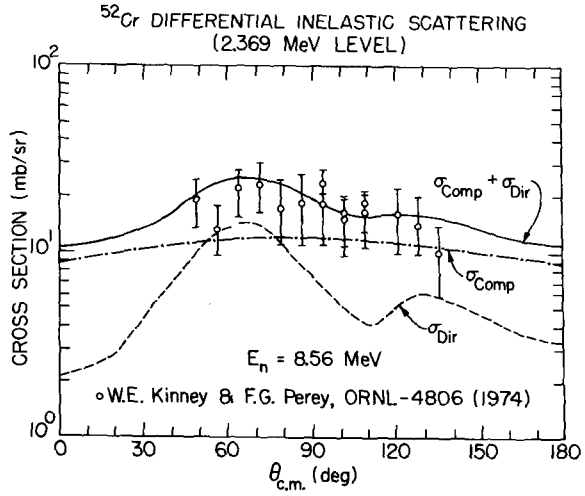

Figure 58.

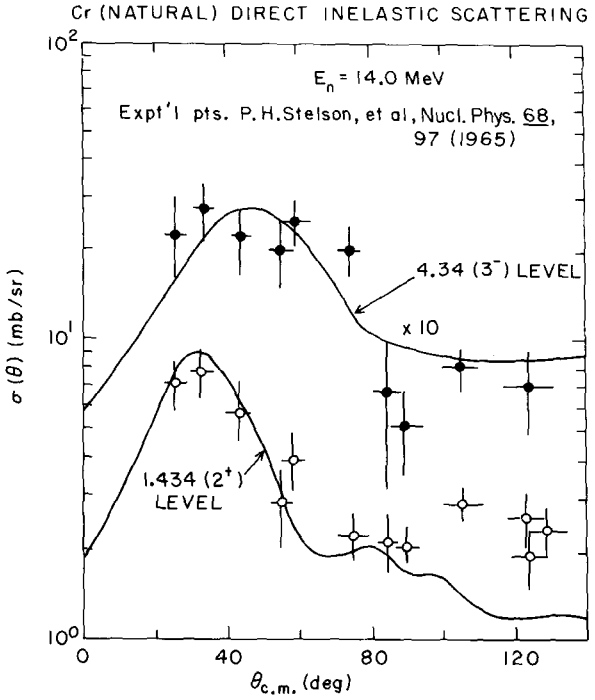

Figure 59.

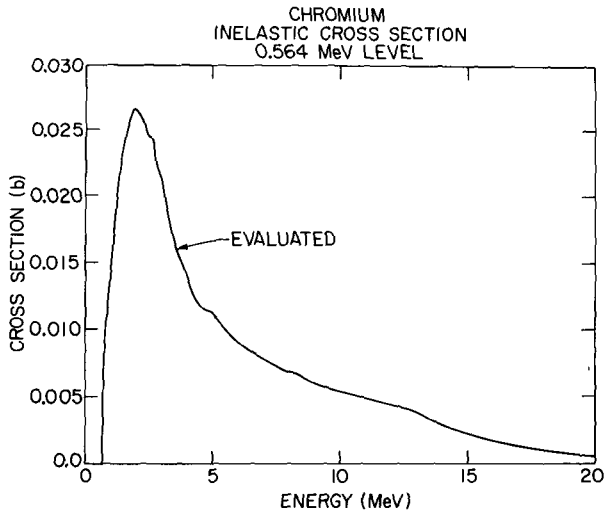

Figure 60.

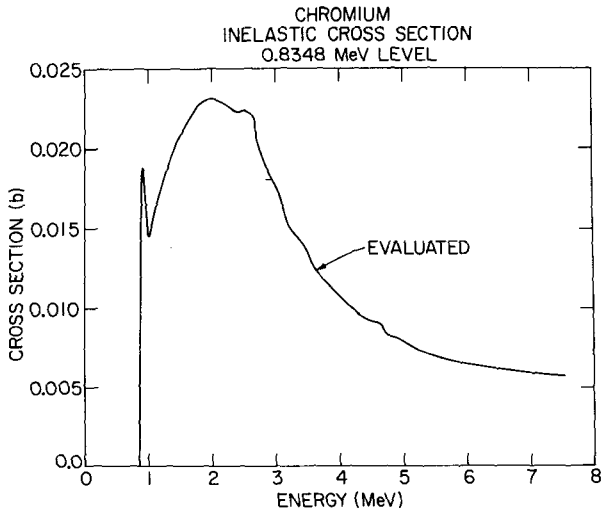

Figure 61.

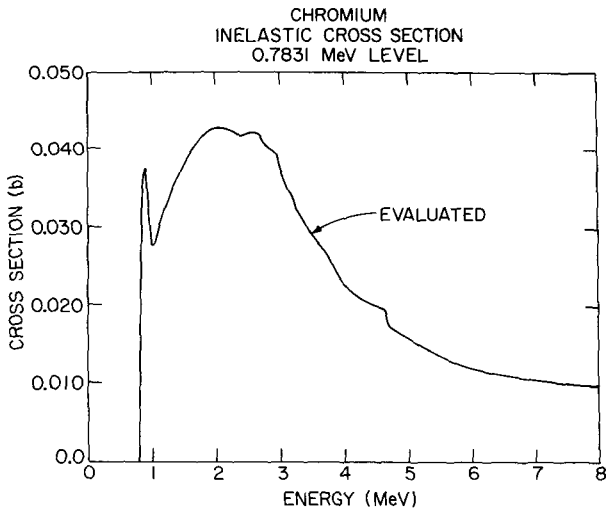

Figure 62.

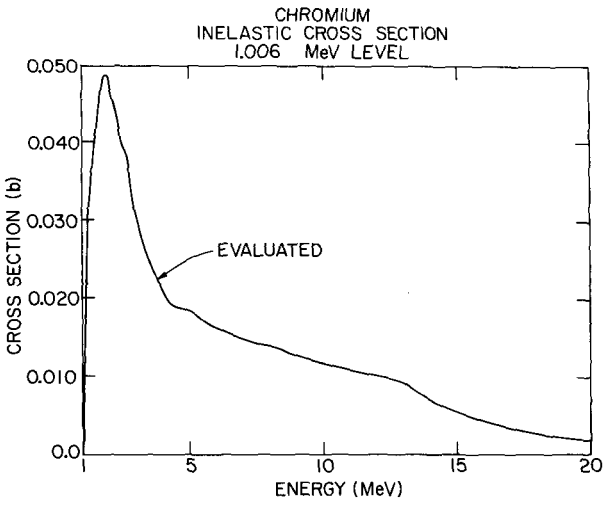

Figure 63.

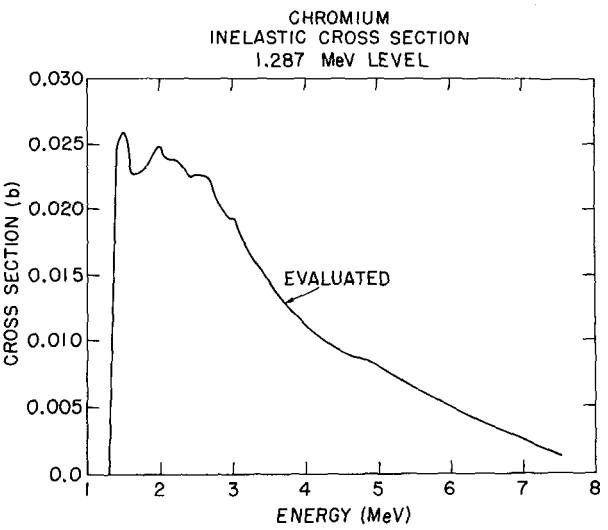

Figure 64.

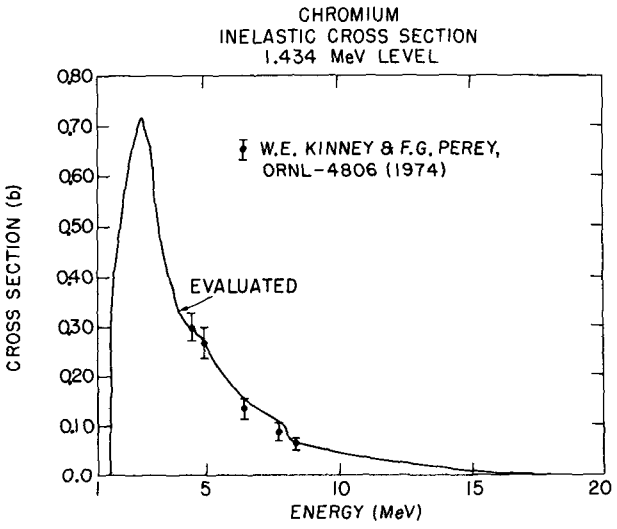

Figure 65.

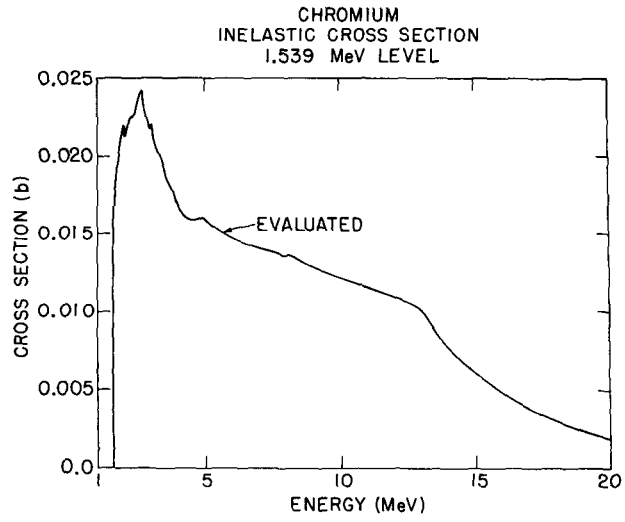

Figure 66.

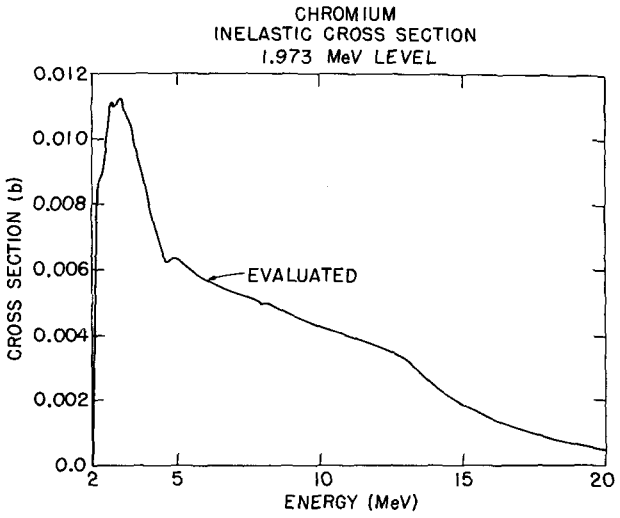

Figure 67.

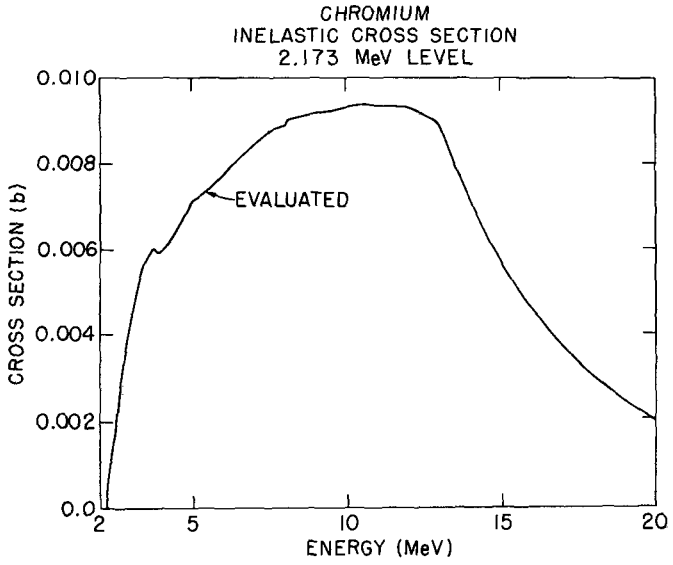

Figure 68.

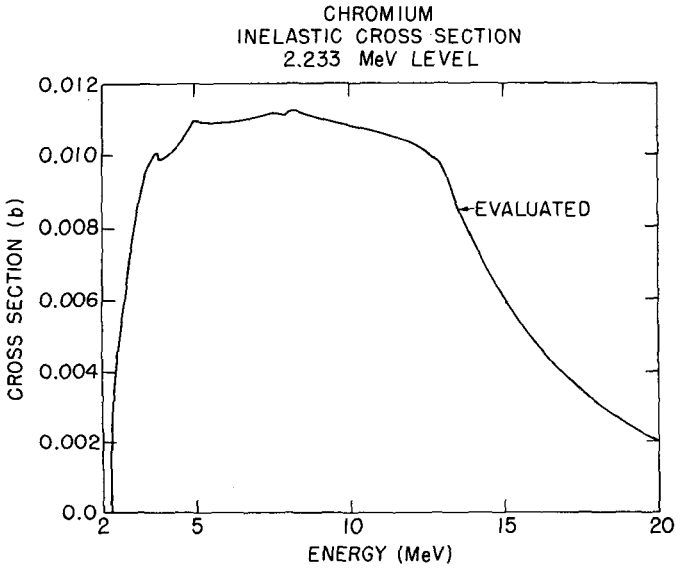

Figure 69.

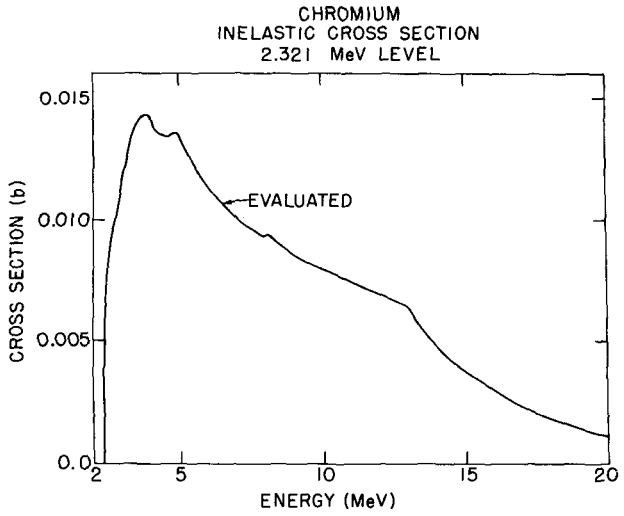

Figure 70.

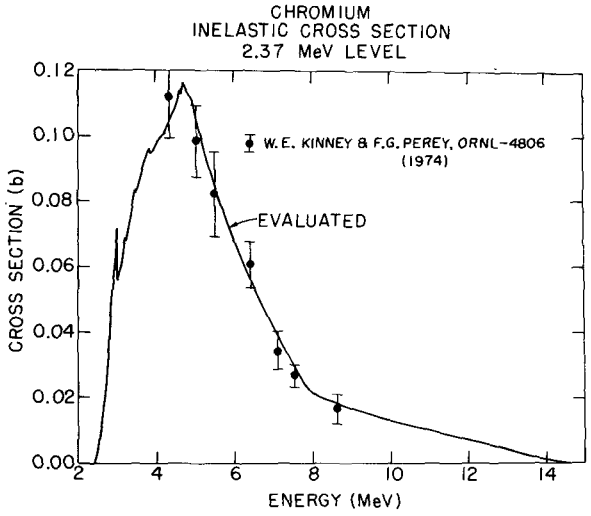

Figure 71.

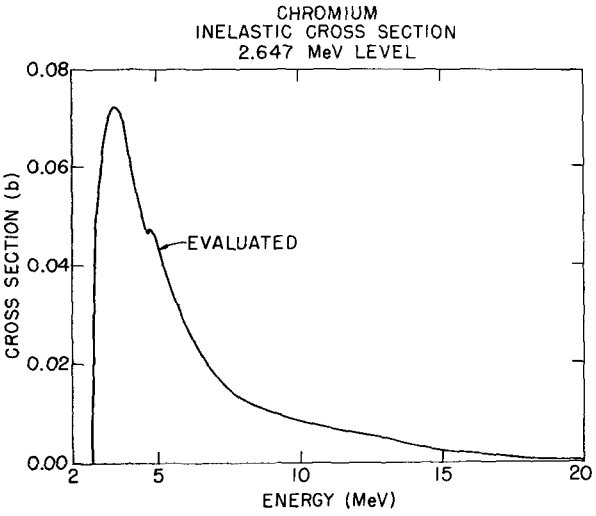

Figure 72.

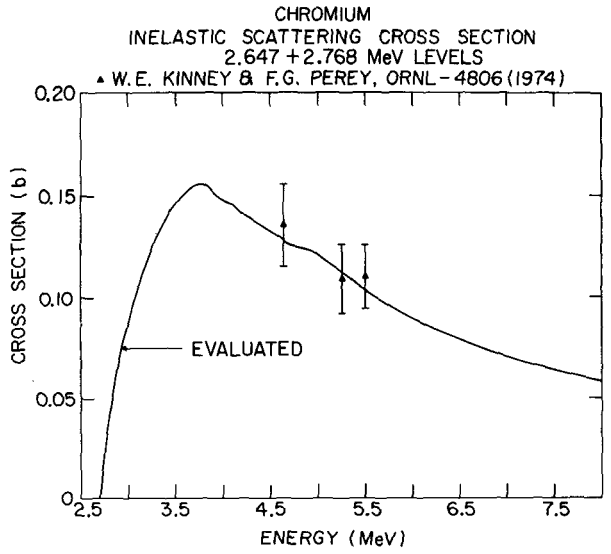

Figure 73.

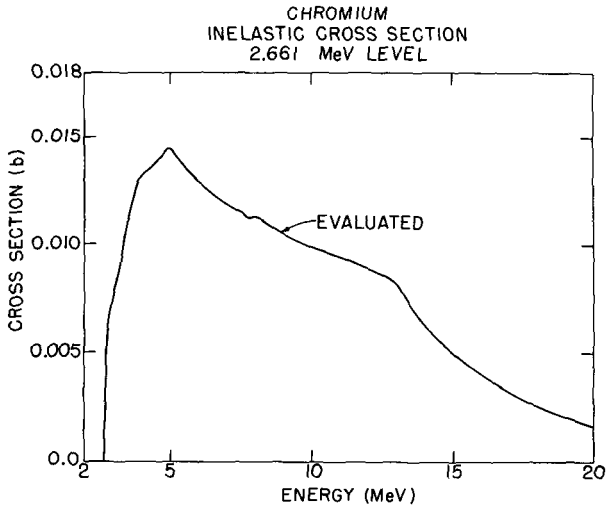

Figure 74.

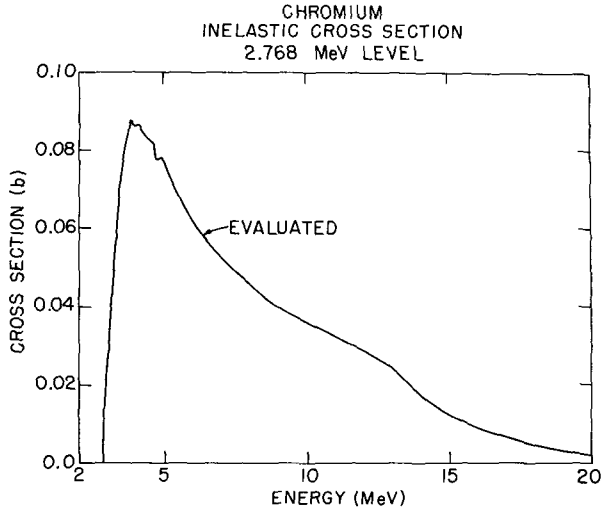

Figure 75.

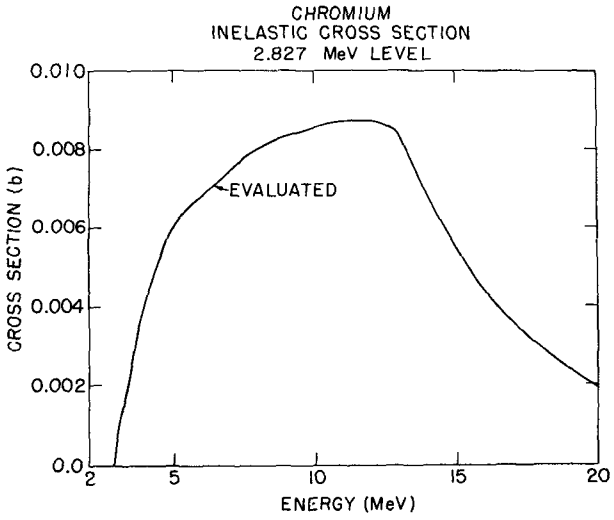

Figure 76.

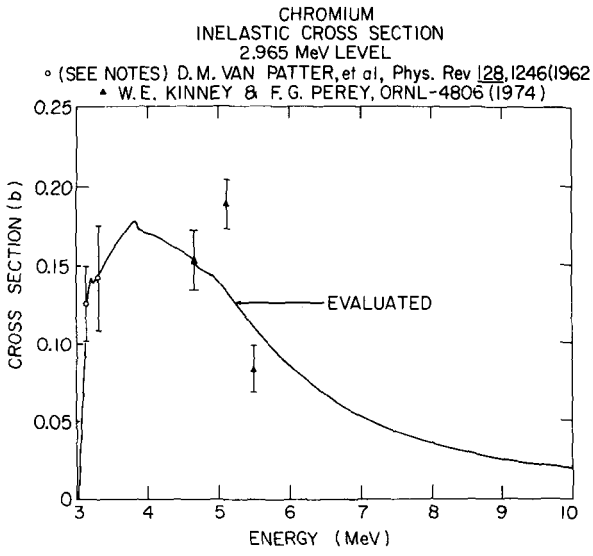

Figure 77.

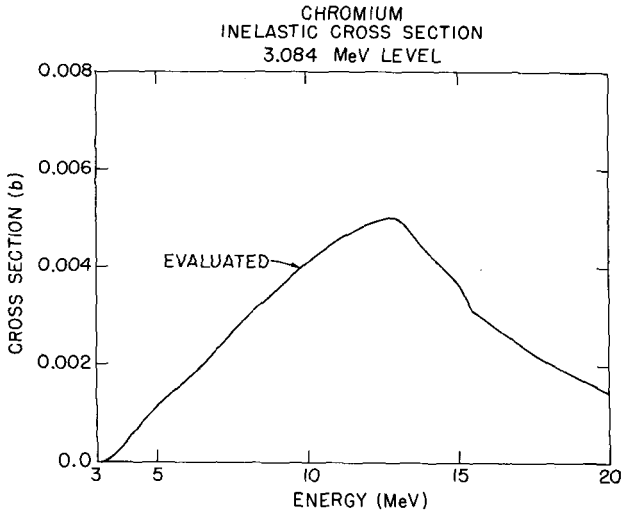

Figure 78.

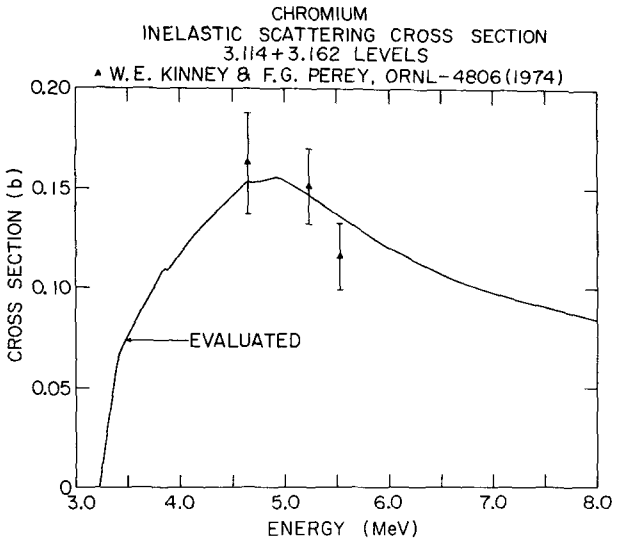

Figure 79.

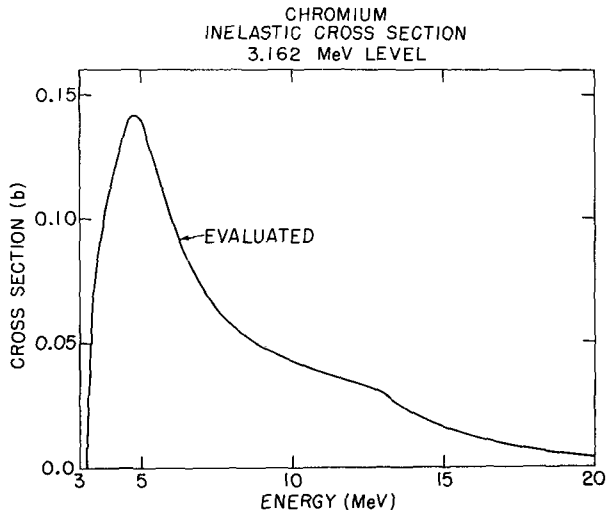

Figure 80.

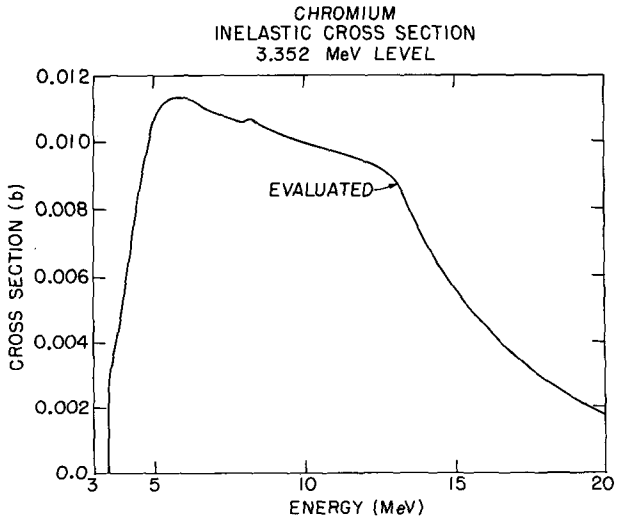

Figure 81.

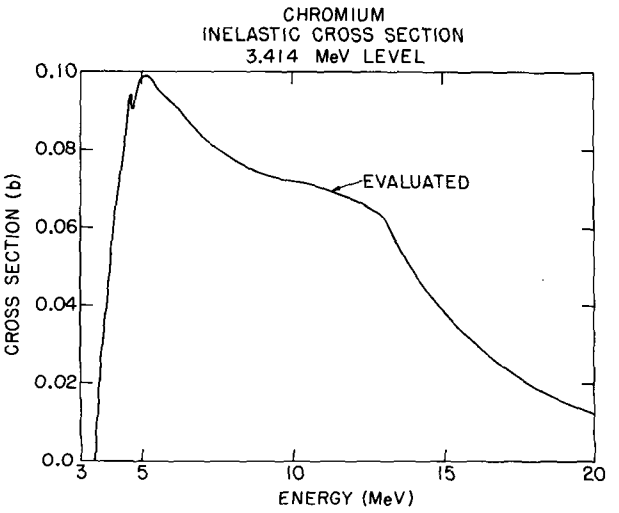

Figure 82.

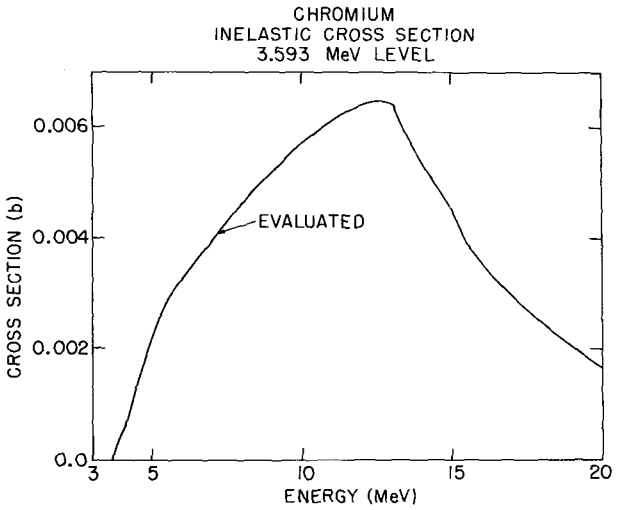

Figure 83.

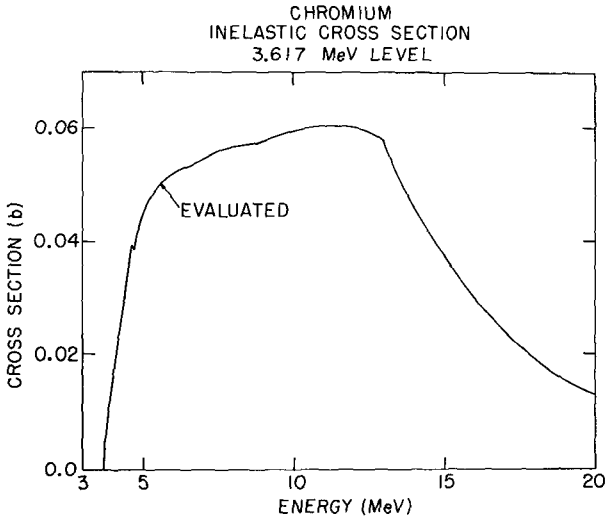

Figure 84.

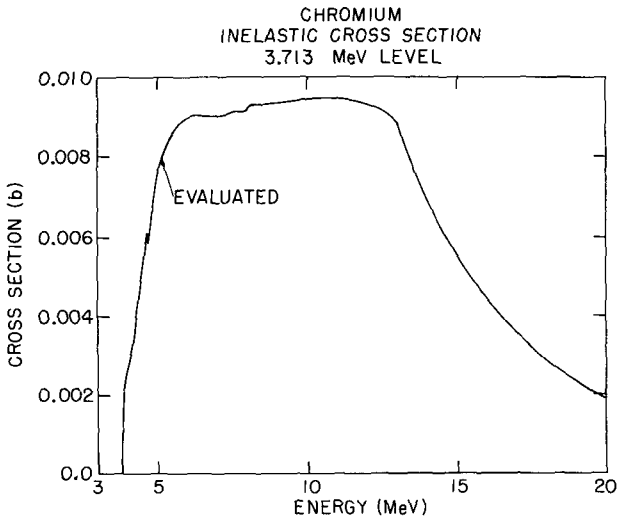

Figure 85.

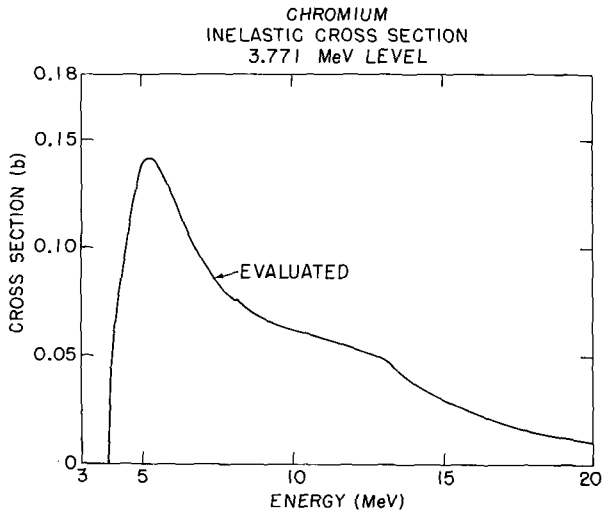

Figure 86.

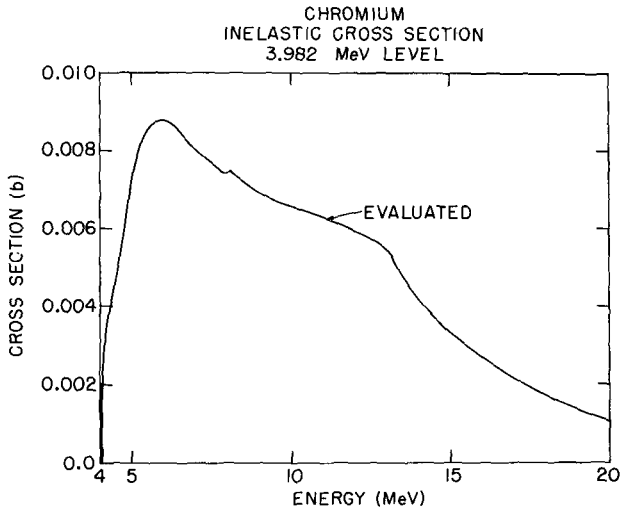

Figure 87.

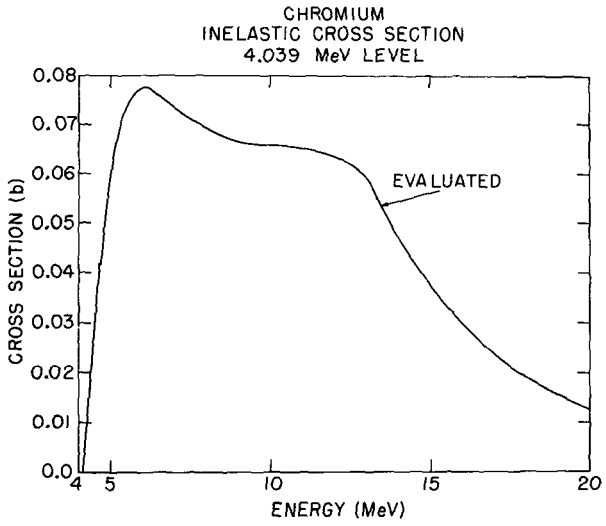

Figure 88.

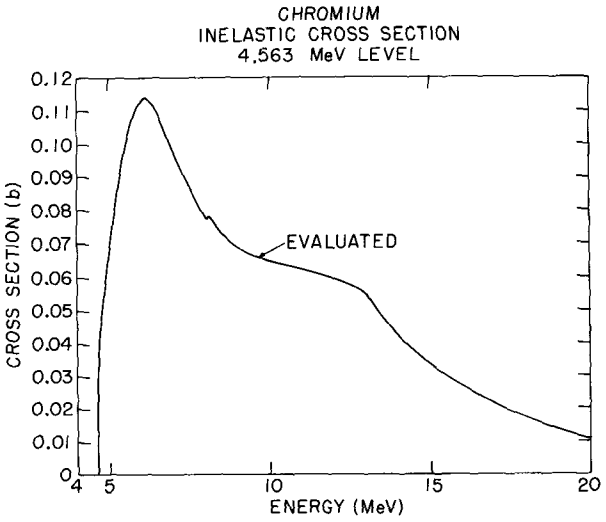

Figure 89.

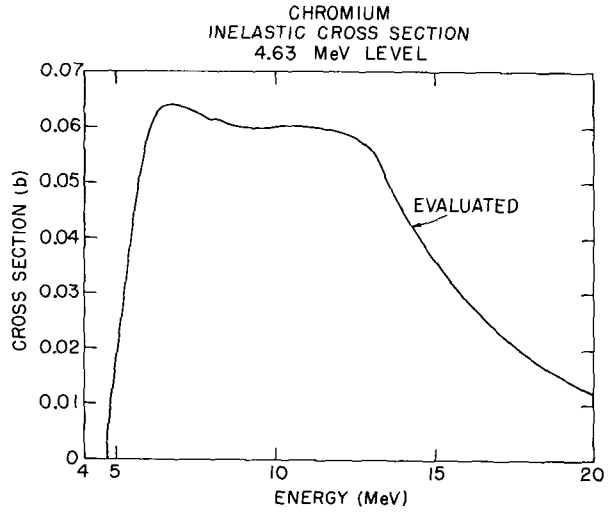

Figure 90.

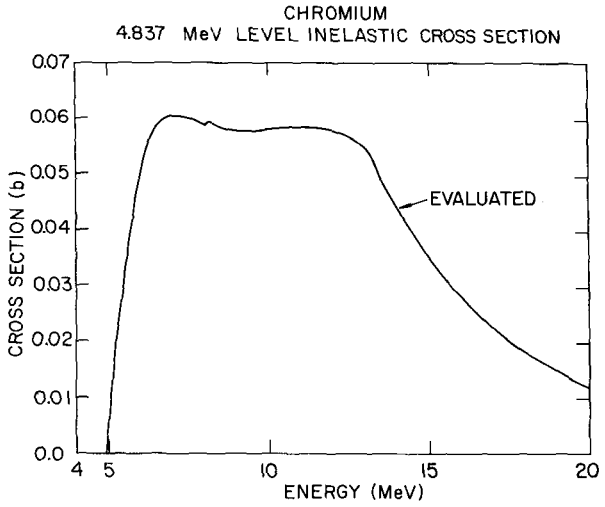

Figure 91.

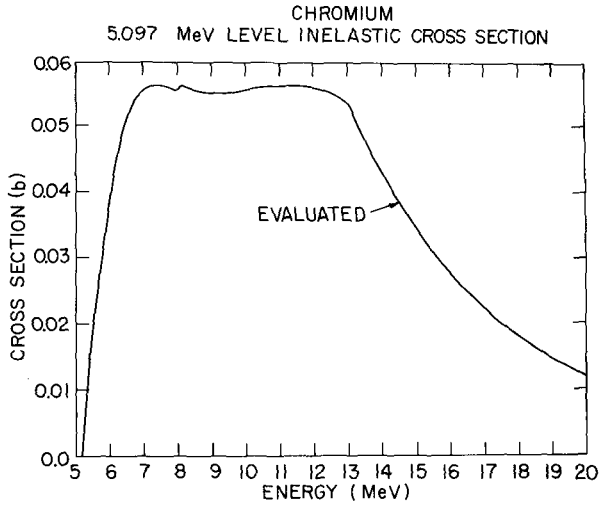

Figure 92.

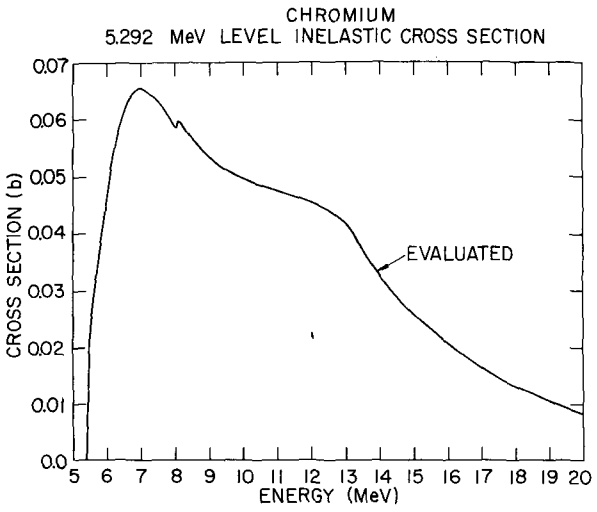

Figure 93.

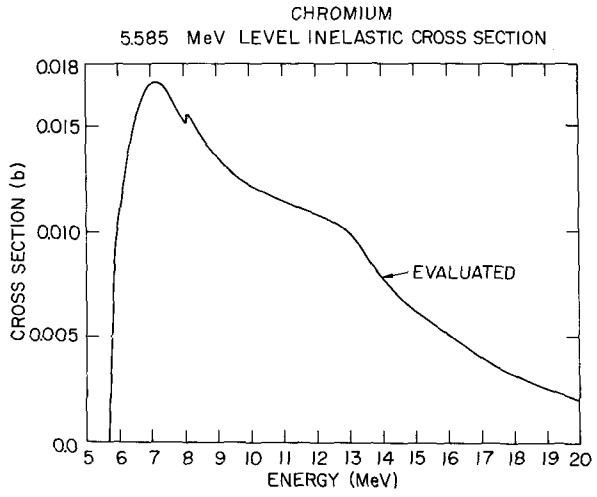

Figure 94.

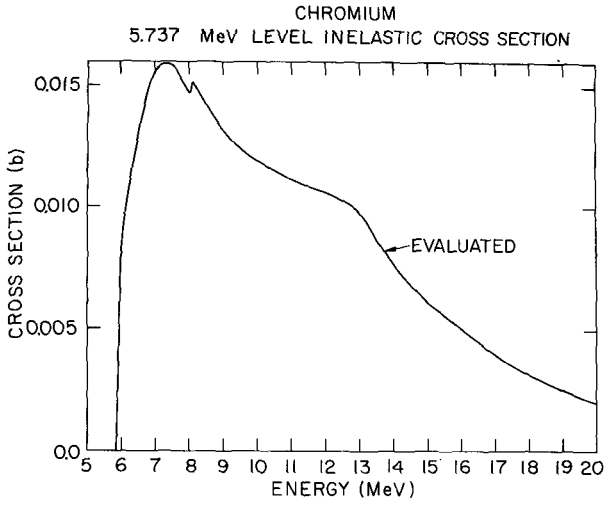

Figure 95.

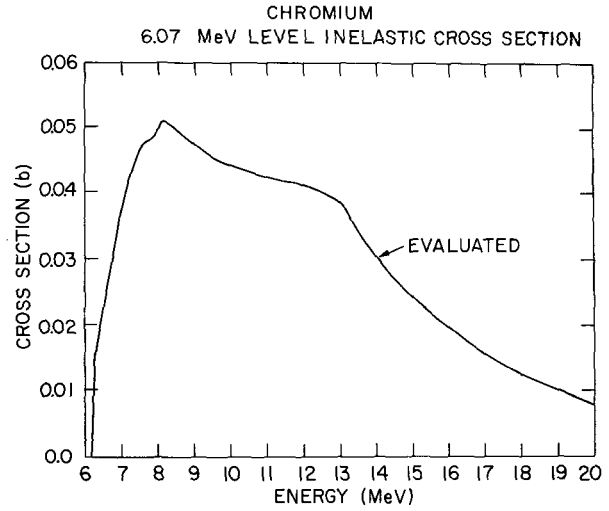

Figure 96.

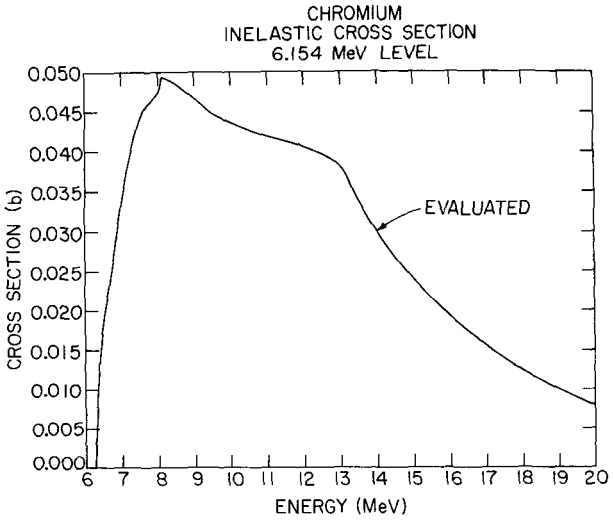

Figure 97.

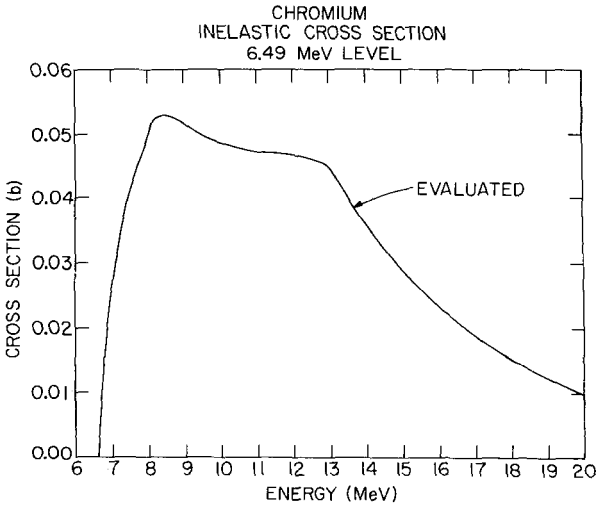

Figure 98.

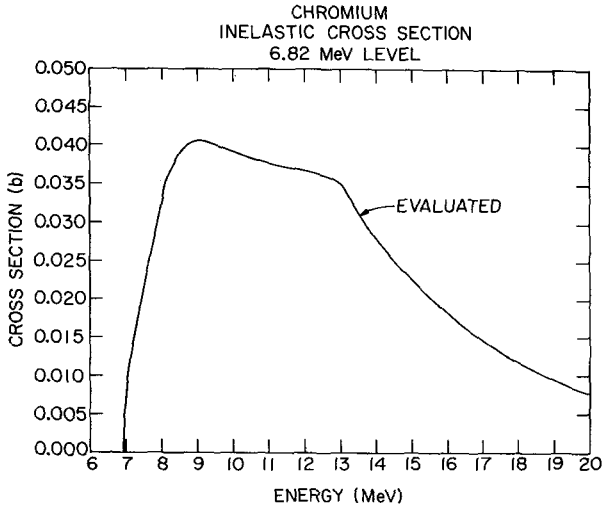

Figure 99.

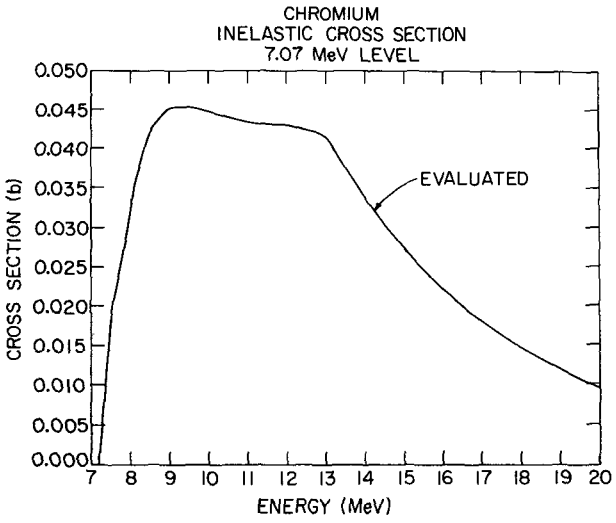

Figure 100.

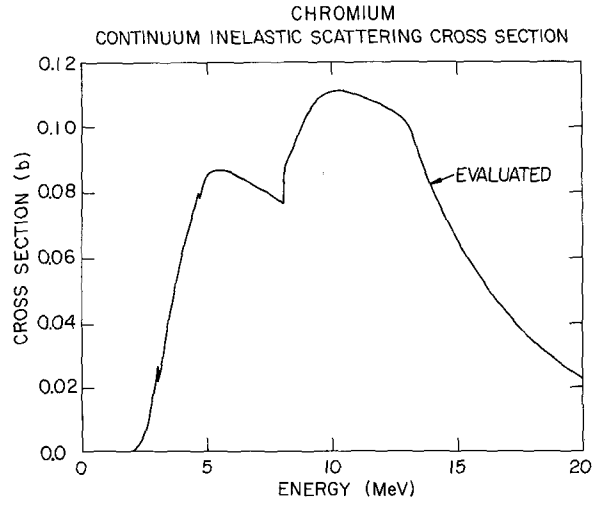

Figure 101.

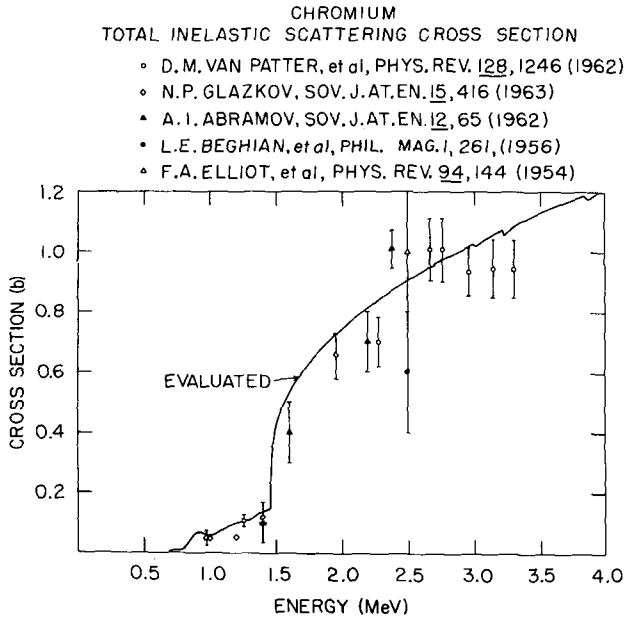

Figure 102.

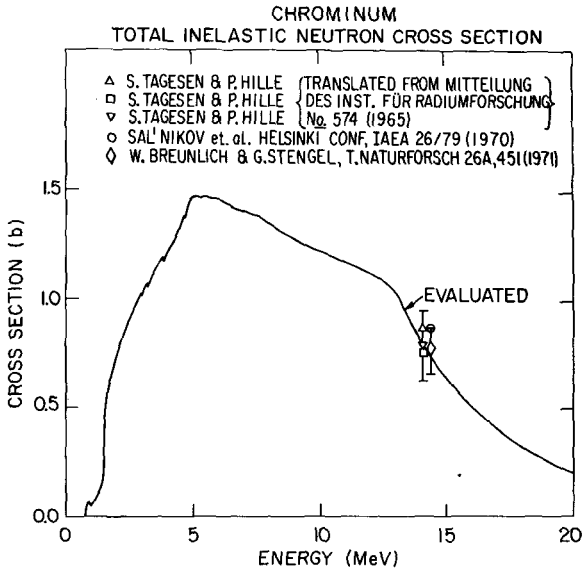

Figure 103.

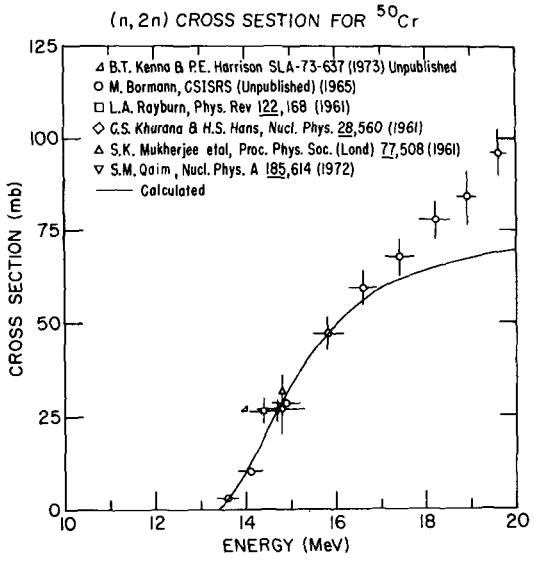

Figure 104.

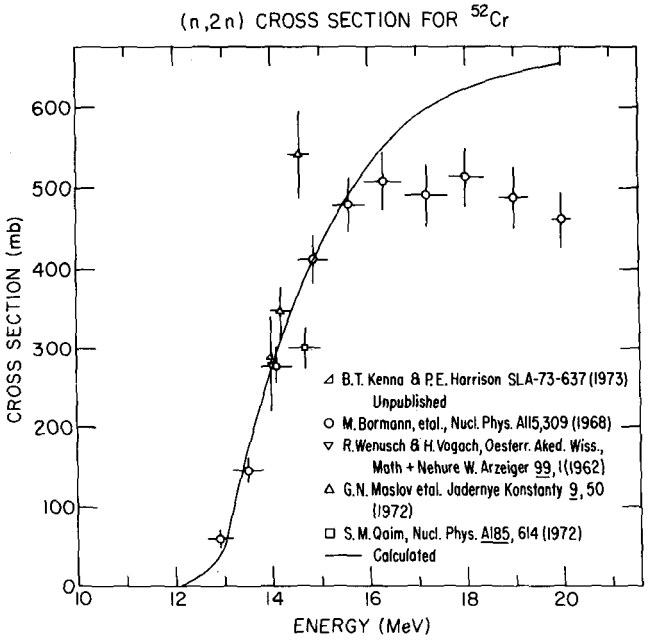

Figure 105.

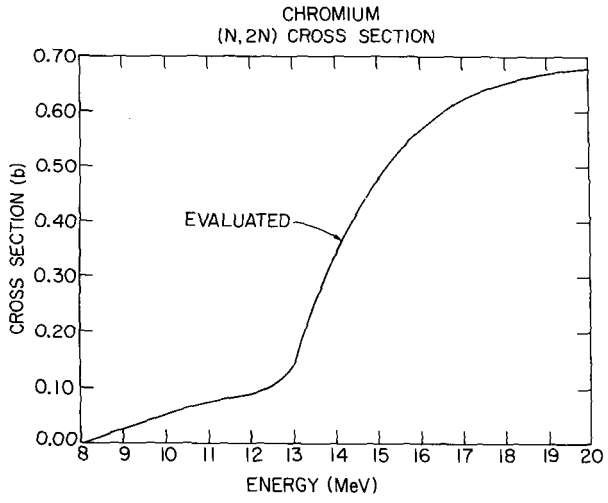

Figure 106.

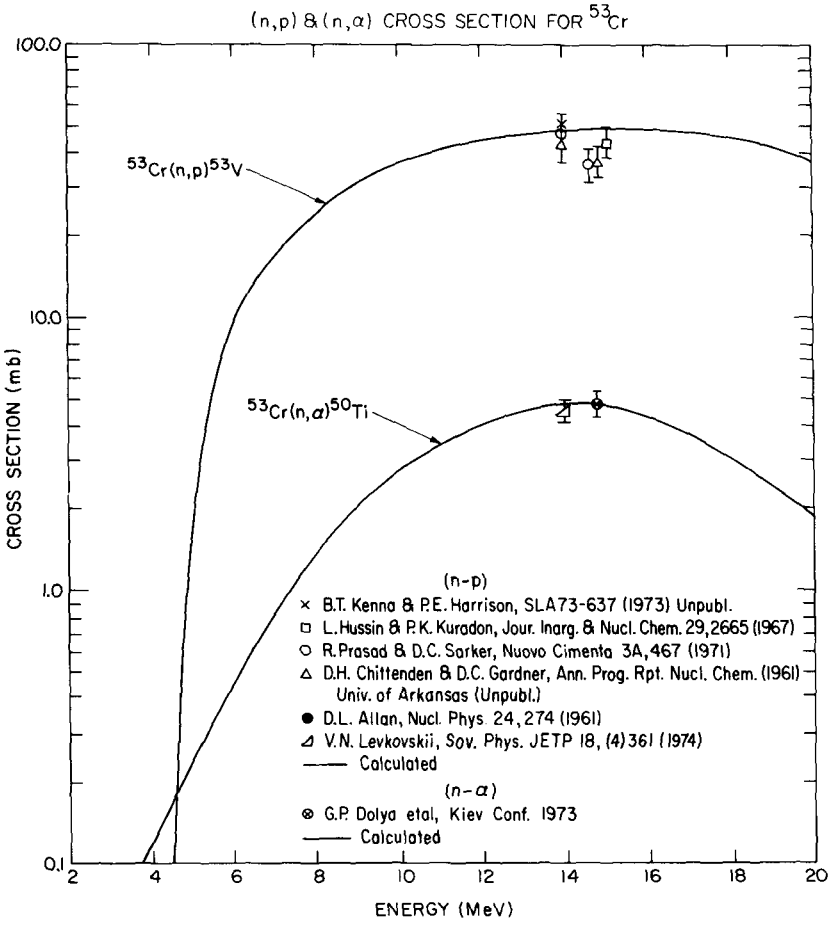
(n,p) & (n,α) CROSS SECTION FOR ^{53}Cr
100.0
10.0
1.0
0.1
CROSS SECTION (mb)
^{53}Cr(n,p)^{53}V
^{53}Cr(n,α)^{50}Ti
(n-p)
× B.T. Kenna & P.E. Harrison, SLA73-637 (1973) Unpubl.
□ L. Hussin & P.K. Kuradon, Jour. Inarg. & Nucl. Chem. 29,2665 (1967)
○ R. Prasad & D.C. Sarker, Nuovo Cimenta 3A,467 (1971)
△ D.H. Chittenden & D.C. Gardner, Ann. Prog. Rpt. Nucl. Chem. (1961) Univ. of Arkansas (Unpubl.)
● D.L. Allan, Nucl. Phys. 24,274 (1961)
◿ V.N. Levkovskii, Sov. Phys. JETP 18, (4) 361 (1974)
—— Calculated
(n-α)
⊗ G.P. Dolya etal, Kiev Conf. 1973
—— Calculated
2
4
6
8
10
12
14
16
18
20
ENERGY (MeV)

Figure 107.

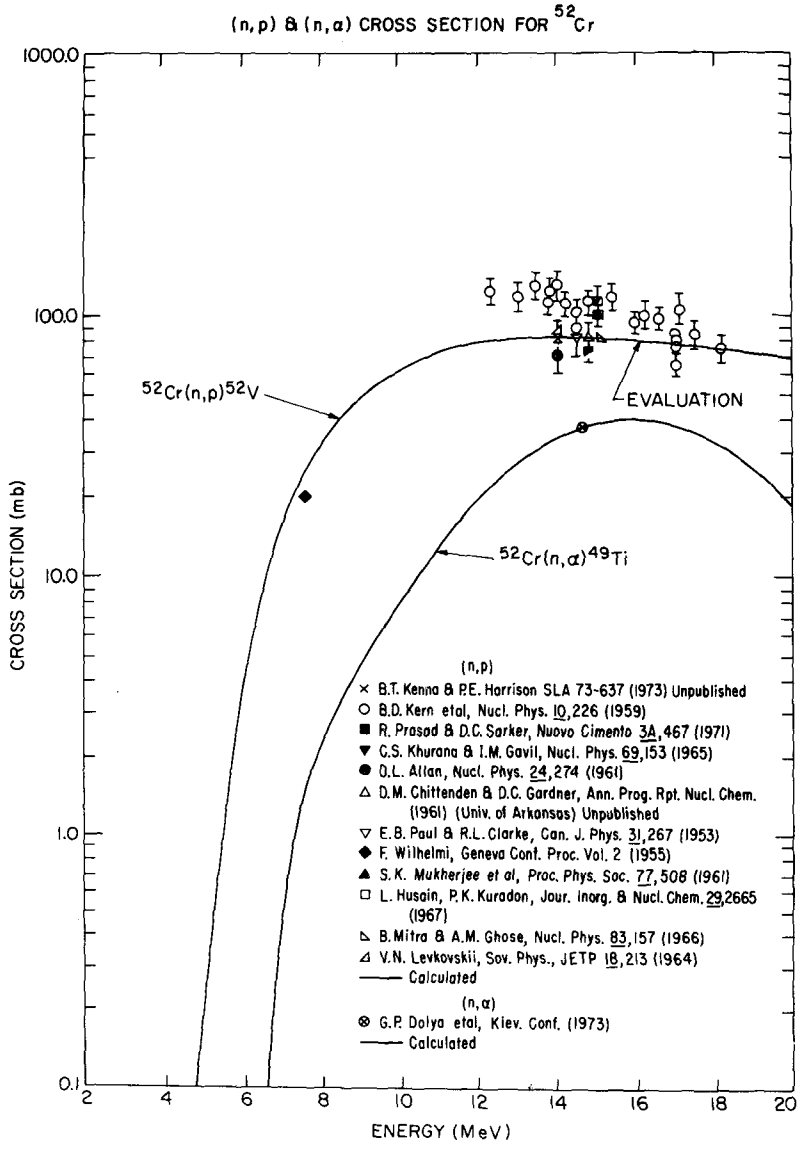
(n,p) & (n,α) CROSS SECTION FOR ^{52}Cr
1000.0
100.0
10.0
1.0
0.1
CROSS SECTION (mb)
2
4
6
8
10
12
14
16
18
20
ENERGY (MeV)
$^{52}Cr(n,p)^{52}V$
EVALUATION
$^{52}Cr(n,\alpha)^{49}Ti$
(n,p)
× B.T. Kenna & P.E. Harrison SLA 73-637 (1973) Unpublished
○ B.D. Kern etal, Nucl. Phys. 10,226 (1959)
■ R. Prasad & D.C. Sarker, Nuovo Cimento 3A,467 (1971)
▼ G.S. Khurana & I.M. Gavil, Nucl. Phys. 69,153 (1965)
● D.L. Allan, Nucl. Phys. 24,274 (1961)
△ D.M. Chittenden & D.C. Gardner, Ann. Prog. Rpt. Nucl. Chem. (1961) (Univ. of Arkansas) Unpublished
▽ E.B. Paul & R.L. Clarke, Can. J. Phys. 31,267 (1953)
◆ F. Wilhelmi, Geneva Conf. Proc. Vol. 2 (1955)
▲ S.K. Mukherjee et al, Proc. Phys. Soc. 77,508 (1961)
□ L. Husain, P.K. Kuradon, Jour. Inorg. & Nucl. Chem. 29,2665 (1967)
◺ B. Mitra & A.M. Ghose, Nucl. Phys. 83,157 (1966)
◿ V.N. Levkovskii, Sov. Phys., JETP 18,213 (1964)
—— Calculated
(n,α)
⊗ G.P. Dolya etal, Kiev. Conf. (1973)
—— Calculated

Figure 108.

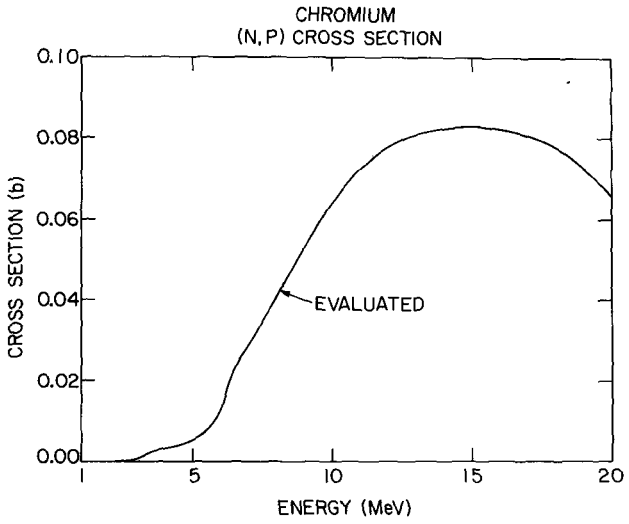

Figure 109.

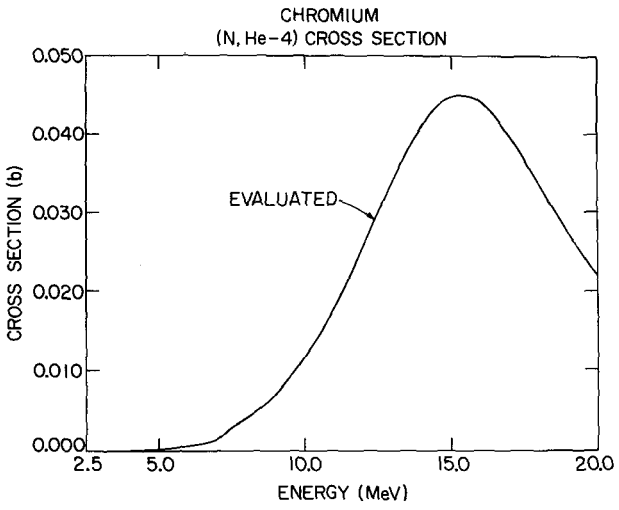

Figure 110.

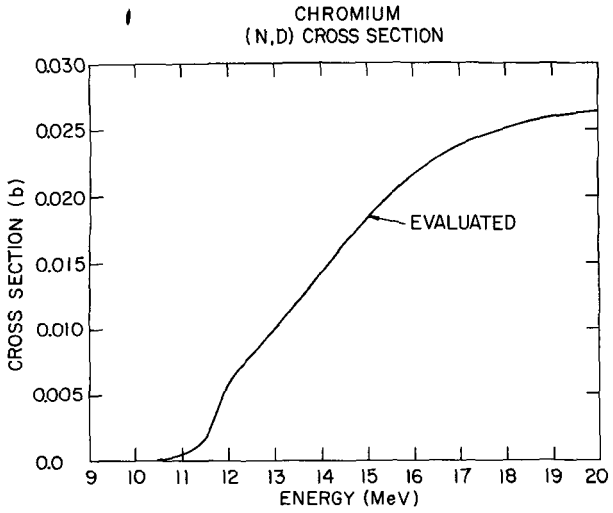

Figure 111.

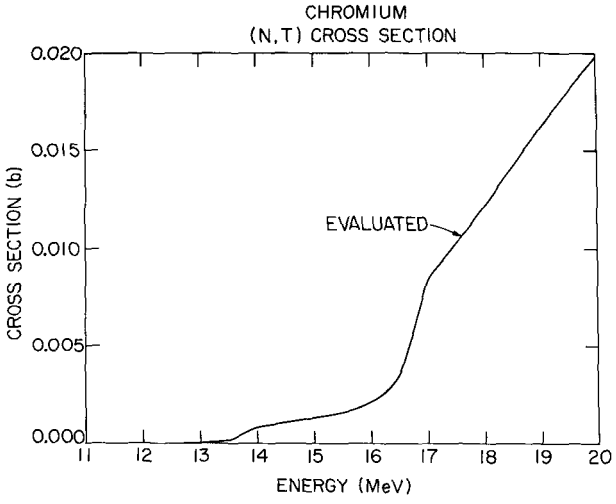

Figure 112.

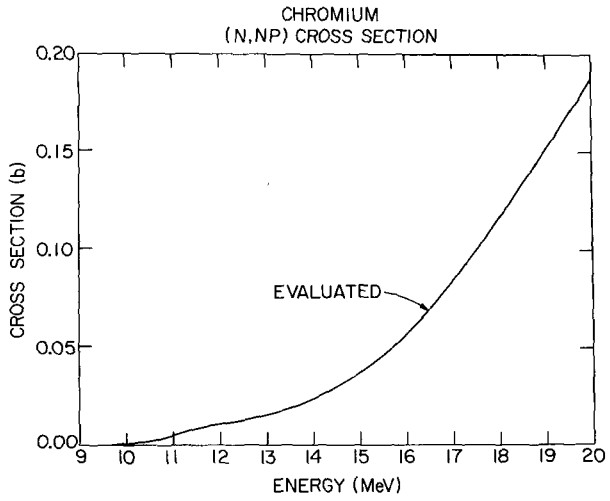

Figure 113.

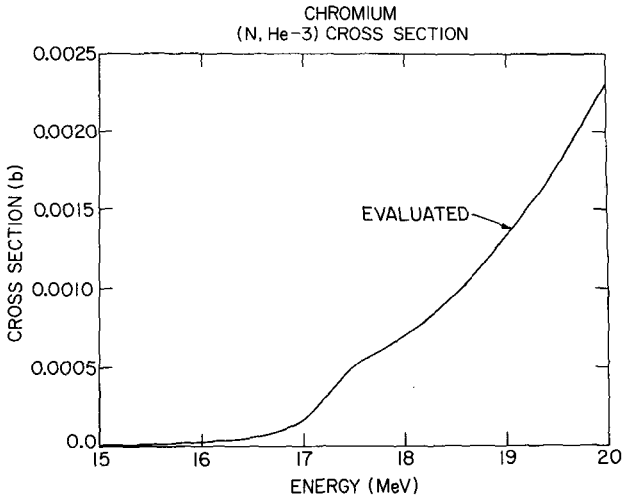

Figure 114.

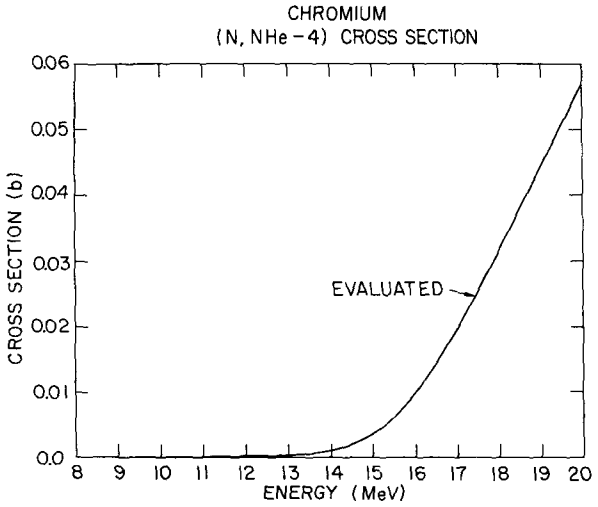
CHROMIUM
(N, NHe-4) CROSS SECTION
CROSS SECTION (b)
0.06
0.05
0.04
0.03
0.02
0.01
0.0
EVALUATED
8 9 10 11 12 13 14 15 16 17 18 19 20
ENERGY (MeV)

Figure 115.

J. R. STEHN

APR 21 1977